



# Microscopic and Acoustic Interpretations of the Physics of Rock Burst and the Difference in Fracturing Patterns in Class I and Class II Rocks

Wenkai Wan<sup>1</sup> · Charlie C. Li<sup>1</sup>

Received: 18 October 2021 / Accepted: 19 July 2022 / Published online: 20 August 2022  
© The Author(s) 2022

## Abstract

The progressive microcracking processes in a burst-prone Class II rock, Kuru granite, and a non-burst-prone Class I rock, Fauske marble were investigated, aiming to reveal the physics of rock burst and the difference in burst-proneness in Class I and Class II rocks. The cylindrical rock specimens of Kuru granite and Fauske marble were uniaxially loaded to various levels in both pre- and post-peak stages, which was monitored by Acoustic emission technique. After that, the thin sections parallel and perpendicular to the loading direction were prepared from each unloaded specimen. The observed intergranular and intragranular cracks in thin sections were quantitatively analyzed in their length, width and orientation as well as the fracturing modes. It was found that extensional intergranular cracking dominated the damaging process in Kuru granite in the pre-peak stage. In the post-peak stage, both intergranular and intragranular cracks increased abruptly. The granite specimen finally failed in splitting. Intragranular shear cracking in calcite dominated the damaging process in Fauske marble. A number of shear fractures formed in the marble and finally the marble failed along a shear fracture zone. It was deduced that, under low confining stress, the fracturing process in Kuru granite of Class II was dominated by extensional fracturing in the direction of  $\sigma_1$ , which dissipated a relatively small portion of the strain energy in the rock and the remaining energy was released for rock ejection. The fracturing in Fauske marble of Class I was dominated by intragranular shear cracking, which dissipated the entire strain energy.

## Highlights

- The fracturing characteristics of Class I and Class II rocks, among others, the predominant cracking orientations and crack density, were microscopically studied during uniaxial compressive loading.
- The inter- and intragranular cracks are quantitatively analyzed in their length, width and orientation as well as the fracture modes.
- The dominant microcracking pattern is intergranular and extensional in the Kuru granite (Class II), but is intragranular and shear in the Fauske marble (Class I).

**Keywords** Extensional cracking · Shear cracking · Microscopic observation · Acoustic emission · Strain burst

## List of Symbols

$\zeta(\theta)$  Total projection length of the cracks in the thin section in the orientation of  $\theta$ , m  
 $\zeta(\theta)_{max}$  Maximum total projection length of the cracks in the thin section, m

$\zeta(\theta)_{min}$  Minimum total projection length of the cracks in the thin section, m  
 $\sigma_1$  Major principal stress, MPa  
 $\phi$  Diameter of the cylindrical core rock specimen, mm  
 $\omega$  Orientation factor of the crack propagation  
 $A$  Area of the thin section, mm<sup>2</sup>  
 $A_i$  Opening area of the  $i$ th crack ( $i = 1, \dots, n$ ) in the thin section, mm<sup>2</sup>  
 $D$  Crack density in the thin section, /mm  
 $E$  Elastic modulus of rock

✉ Charlie C. Li  
charlie.c.li@ntnu.no

<sup>1</sup> Department of Geoscience and Petroleum, NTNU  
Norwegian University of Science and Technology,  
Trondheim, Norway

$I$	Intergranular cracks
$L_\theta$	Projection line with an angle, $\theta$ , to the horizontal line
$l_i$	Length of the $i$ th crack ( $i = 1, \dots, n$ ) in the thin section, mm
$RA$	Ratio of the rising time to the amplitude of the AE signal, ms/V
$S\parallel$	Vertical thin section that is parallel with the loading direction
$S\perp$	Horizontal thin section that is perpendicular to the loading direction
$T$	Intragranular cracks
$UCS$	Uniaxial compressive strength of the rock, MPa
$W$	Average opening width of all the cracks in the thin section, $\mu\text{m}$

### Abbreviations

AE	Acoustic emission
CT	Computed tomography
FFT	Fast Fourier transformation
ISRM	International Society for Rock Mechanics
LVDT	Linear variable differential transformer
SEM	Scanning electron microscope

## 1 Introduction

Rock burst is a phenomenon in which rock disintegrates, accompanied by the ejection of a volume of debris (Li 2021). It often occurs in deep underground mines and deep tunnels where in-situ rock stresses are high. Based on the triggering mechanisms, there are two types of rock bursts—strain burst associated with overstressing, and fault-slip burst associated with the slippage of pre-existing faults (Li 2011).

Strain burst will occur when the total strain energy stored in the rock to be ejected and the energy released from the surrounding rock are greater than the energy needed for rock fracturing. The excessive energy is converted into kinetic energy to eject the rock (Li 2019). Rock fracturing and energy conversion are involved in strain burst.

Rocks are classified into Class I or Class II based on the stress–strain behavior of the rocks in the post-peak stage in servo-controlled uniaxial compressive tests (Akinbinu 2016; Fairhurst and Hudson 1999; Hashiba et al. 2006). For Class I rocks, the axial strain (displacement) increases with a decrease in the axial stress after the stress passes the peak value, as shown in Fig. 1a. For Class II rocks, the axial strain has to reverse immediately after the peak stress to maintain the failure of the rock to be progressive and stable, as shown in Fig. 1b. There exists an excess strain energy released from the rock, which is converted to kinetic energy to eject rock. In the reality, Class I rocks fail progressively in the post-peak stage, while Class II rocks fail violently, or in bursting. Class I rocks are typically relatively soft (low  $E$ -modulus) and ductile, such as the Fauske marble used in the tests of this study (Fig. 1a). Class II rocks are brittle and burst-prone, such as the Kuru granite in this study (Fig. 1b).

Rocks are aggregates of different mineral grains. They contain defects and microcracks within and between the constituent mineral grains, as well as textures, such as cleavages. These defects and cleavages are often the nuclei for new crack initiation (Dyskin et al. 2003; Park and Bobet 2010). Rock damage is a process of crack initiation and propagation. A lot of effort has been expended in the development of crack propagation theories (Hoek and Martin 2014; Kemeny and Cook 1987), and in the study of the coalescence process of cracks (Tang and Kou 1998; Zhang and Wong 2013). Advanced technologies such as

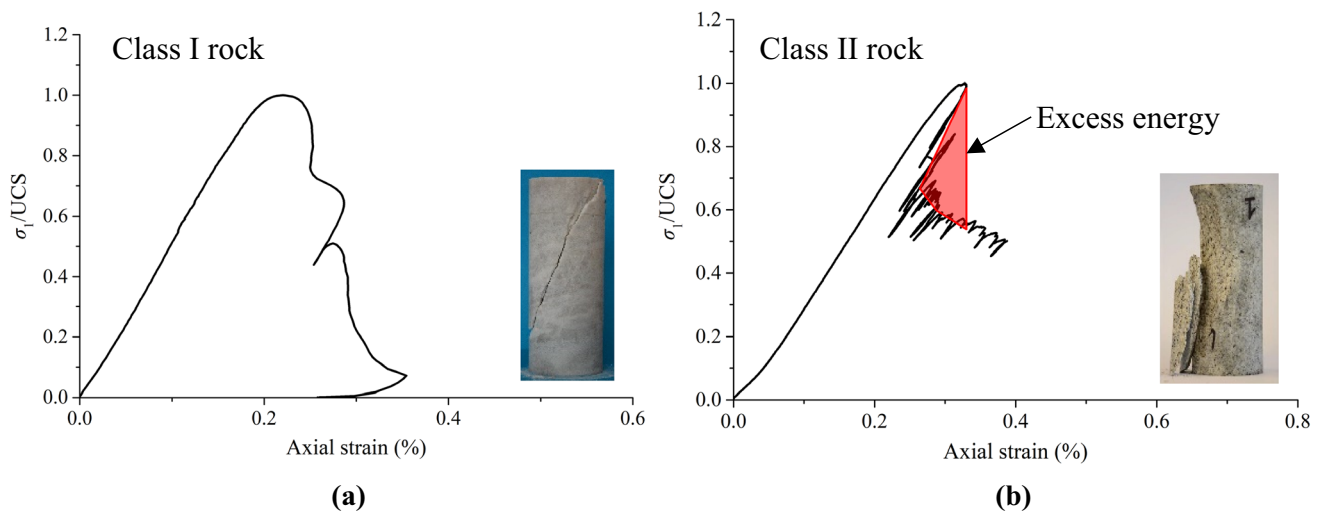


**Fig. 1** Stress–strain curves of the **a** Fauske marble (Class I rock) (Zhang and Li 2019), and **b** Kuru granite (Class II rock) (Tkalic et al. 2016)

CT and SEM have been used for microscopic investigations of fractures in rocks (Fan et al. 2020a, 2020b, Fan et al. 2022). Cracking and deformation of the rock can be divided into five stages—crack closure, elastic deformation, stable crack propagation and coalescence, unstable crack propagation, and ultimate failure (Ghamgosar et al. 2017). Various types of rocks containing different numbers of flaws have been tested extensively (Bobet and Einstein 1998; Brace and Bombolakis 1963; Horii and Nemat-Nasser 1985; Petit and Barquins 1988; Wong and Einstein 2009; Yang et al. 2009). All these studies suggested that two major crack types could initiate from a single pre-existing flaw, namely, extensional crack and shear crack. Extensional cracking occurs in the direction of the major principal stress. The surfaces of extensional cracks are usually clean and rough because the cracks are simply generated via intergranular separations (Bobet and Einstein 1998; Horii and Nemat-Nasser 1985; Whittaker et al. 1992). Extensional cracks do not offset between the surfaces. Extensional cracking is the most common microcracking mode in Class II rocks, such as basalt and strong granite, under uniaxial compression (Tkalich et al. 2016; Zhang et al. 2020). In shear cracking, relative slippage occurs on the crack surfaces. Shear crack surfaces incline in the direction of the major principal stress at an angle ranging from 10° to 30°. Shear cracks are often smooth and filled with finely ground mineral powders (Bobet and Einstein 1998; Horii and Nemat-Nasser 1985; Whittaker et al. 1992). Shear cracks coalesce to form macroscopic shear fractures, which leads to final failure in the rock. Shear fracturing is the most common failure mode in triaxial compression (Tkalich et al. 2016; Zhang and Li 2019), and may also occur under uniaxial compression in weak rocks (Yang et al. 2008; Zhang and Li 2019). While significant work has been conducted in the macroscopic observation and differentiation of extensional and shear cracks, only few studies focused on investigating these two crack types in the microscopic scale. Those studies were mostly interested in the surface features of microcracks instead of comparing the extensional and shear cracks in detail (He et al. 2015). It is believed that extensional cracking is mainly related to intergranular cracks, while shear cracking is related to intragranular cracks (Cheng and Wong 2018). Intergranular or intragranular cracks are easy to be distinguished in optical microscopic studies. However, the progressive developments of intergranular cracks and intragranular cracks involved in the extensional and shear cracks have been seldom studied quantitatively. Although the considerable research has been widely reported on cracking behaviors and failure processes in Class I and Class II rocks (He et al. 1990; Janach 1977; Labuz and Biolzi 1991; Pan et al. 2006; Tarasov and Stacey 2017; Wang et al. 2020), they did not explain the reasons why

Class I and Class II rocks have different failure characteristics and burst-proneness from a micro perspective. The heart of rock burst—the physics is not clear so far. The influence of the development of different types of microcracks on the generation and propagation of macroscopic cracks and the energy dissipation, and the influence on the burst-proneness of two rock classes need to be further understood.

This study focused on the microcracking processes and final failure modes in both the burst-prone Kuru granite and non-burst-prone Fauske marble. The aim of the study was to reveal the physics of burst-prone Class II rock and the difference in microcracking features in Class I and Class II rocks based on the observations and measurements on the Kuru granite and the Fauske marble. In the study, the microcracks in the rock specimens were examined in terms of their types (intergranular or intragranular), propagation direction and dimensions (length and opening width) on an optical microscope after the specimens were uniaxially loaded to different stress levels in both the pre-peak and post-peak stages. The crack networks in the specimens were quantitatively described in terms of crack density, average opening width and orientation factor. The cracking patterns were compared with the characteristics of the acoustic emissions (AEs) recorded during testing.

## 2 Laboratory Testing

The rock specimen tests were conducted in three steps: (1) uniaxial compression of the specimen to a certain load level; (2) thin section cutting; and (3) microscopic observation, as illustrated in Fig. 2.

### 2.1 Materials and Specimens

Kuru granite (quarried in Kuru, Finland) and Fauske marble (quarried in Fauske, Norway) were used in this study. The Fauske marble and the Kuru granite are typical Class I and Class II rocks based on a long time of previous studies in our and others' laboratories (e.g. Fourmeau et al. 2014, 2017; Herman and White 1985; Hokka et al. 2016; Saksala et al. 2013, 2014; Tkalich et al. 2016; Zhang and Li 2019). Kuru granite is mainly composed of quartz, intermediate albite and microcline, while Fauske marble is formed of 99% calcite crystals with only a small amount of impurities, as shown in Fig. 3. Microscopic observations of the intact rocks revealed their inherent grain structures (Fig. 4). The different mineral grains in the Kuru granite were squeezed into each other with bumpy contacts, forming an interlocking structure (Fig. 4a). The Fauske marble was characterized by a mutually interfering growth pattern and a well-fused interlocking polygonal granoblastic texture (Fig. 4b). A few

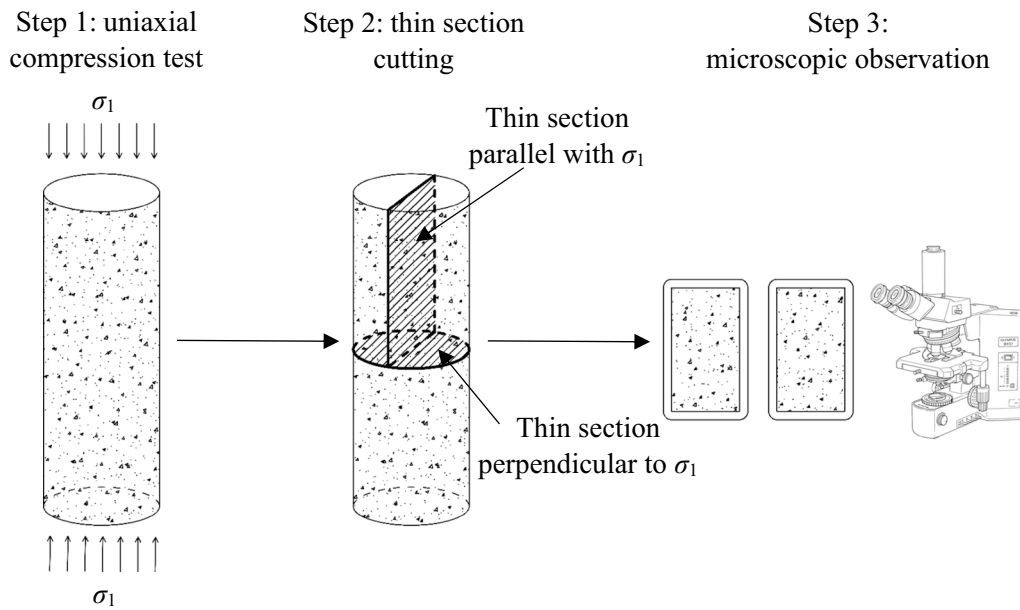


**Fig. 2** Experimental procedure: Step 1—uniaxial compression of the rock specimen; Step 2—thin section cutting; and Step 3—microscopic observation

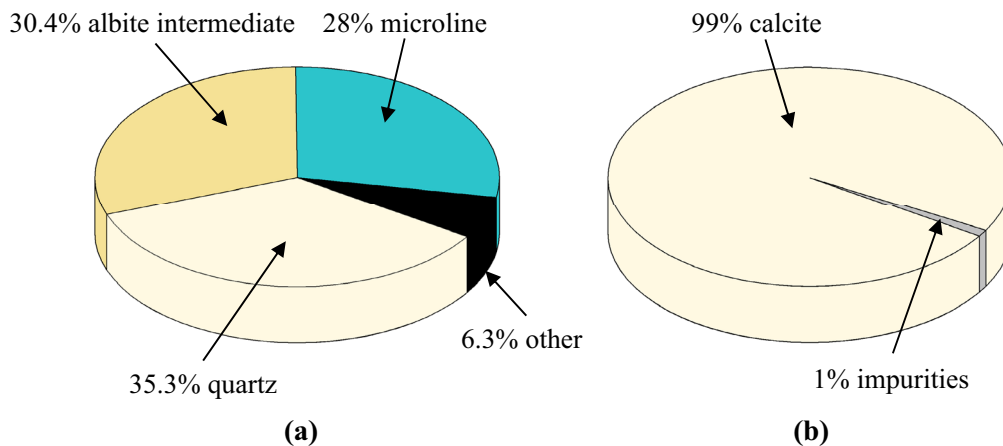


**Fig. 3** Mineral compositions of the **a** Kuru granite, and **b** Fauske marble

microcracks and voids were present. Prominent sets of twin cleavages were also observed in most of the grains in the Fauske marble. It was found that intragranular cracks were predominantly nucleated in these twin lamellae.

A total of six cylindrical core specimens, each  $\phi$  49 × 133 mm, were prepared for each of the two rock types, using the methods provided by ISRM (Brown 1981). All specimens were dried under ambient temperature conditions. All six specimens of each rock type were drilled from the same cube. Therefore, the mechanical properties of the specimens are identical for each rock type.

## 2.2 Uniaxial Compression Tests

The uniaxial compression tests were conducted on a servo-controlled testing machine (GCTS RTR-4000), which had an axial load capacity of 4000 kN and a frame stiffness of 15 GN/m. The axial and radial strains were measured using linear variable differential transformers (LVDTs), and the data were automatically recorded by an acquisition system. A close-up of a specimen before testing is shown in Fig. 5a. A transparent thermoplastic membrane was wrapped around each specimen to preserve the rock debris. On Fig. 5a, the two thin bars on each side of the specimen, fixed to the black rings, are the LVDTs for axial strain

**Fig. 4** Photomicrographs of the **a** Kuru granite, and **b** Fauske marble in their original states under cross-polarized light. Labeled features: (1) voids in grains and boundaries; (2) microcrack-free boundary; (3) intergranular crack; (4) intragranular crack; and (5) twin lamellae

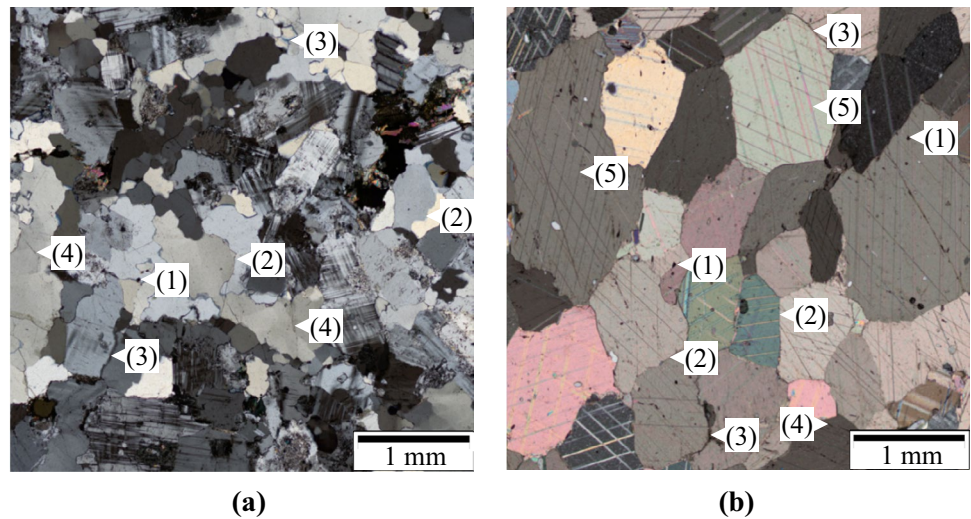
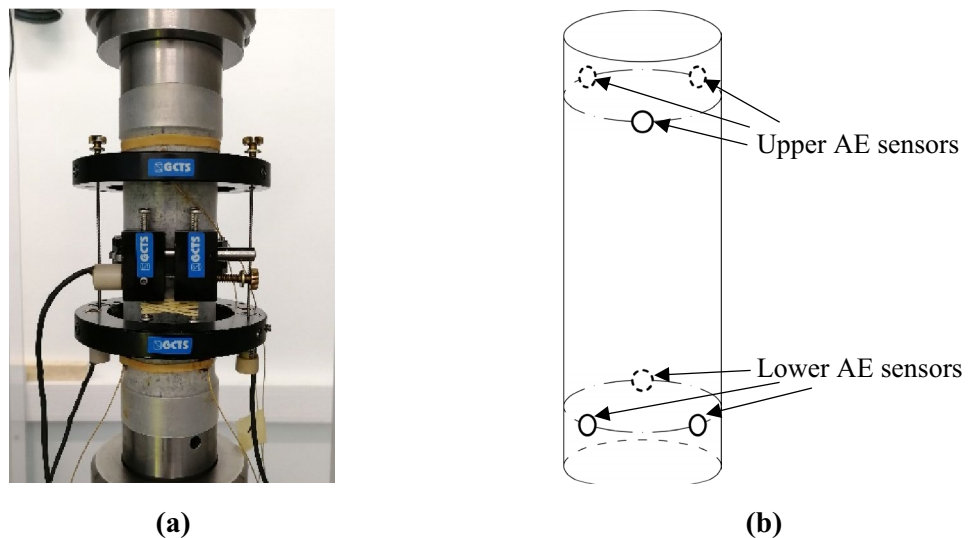


**Fig. 5** **a** Close-up of a specimen prepared for a uniaxial test; and **b** positions of the AE sensors



measurement, while the central rim is the circumferential LVDT for radial strain measurement. Three AE sensors were attached to each end of the specimen at a distance of approximated 15 mm from the ends. The upper and lower AE sensors were staggered at  $60^\circ$  (Fig. 5b). Ultrasonic gel was smeared between the AE sensors and the specimen to improve the acoustic transmission at the interface. A rubber band was used to hold the AE sensors tight against the specimen (Fig. 5a).

All the tests were performed at a room temperature of approximately  $20^\circ\text{C}$ . Each specimen was loaded to a predetermined stress level. The specimens of the granite were first loaded to 55 MPa at a loading rate of 0.8 MPa/s under axial stress control. Then, the loading was switched to radial strain control at a rate of  $250\ \mu\text{e}/\text{min}$ , and gradually increased to  $400\ \mu\text{e}/\text{min}$ . The test remained under radial strain control until failure. The switch from stress control to strain control

at a relatively low stress level was purely an operational measure to guarantee a stable start to the loading. The six granite specimens were loaded to 47% UCS pre-peak, 80% UCS pre-peak, peak stress, 90% UCS post-peak, 75% UCS post-peak and 57% UCS post-peak, respectively, where 'UCS' represents the uniaxial compressive strength of the rock. For the marble specimens, the axial stress was applied at a rate of  $18\ \mu\text{e}/\text{s}$  under axial strain control up to peak stress. Then the axial strain rate was lowered to  $14\ \mu\text{e}/\text{s}$  for the rest of the test to capture the post-peak behavior. The six marble specimens were loaded to 44% UCS pre-peak, 79% UCS pre-peak, peak stress, 80% UCS post-peak, 59% UCS post-peak and complete failure, respectively. The specimen was unloaded once the target stress level was reached. AE technique was used to monitor the progressive fracturing during loading.

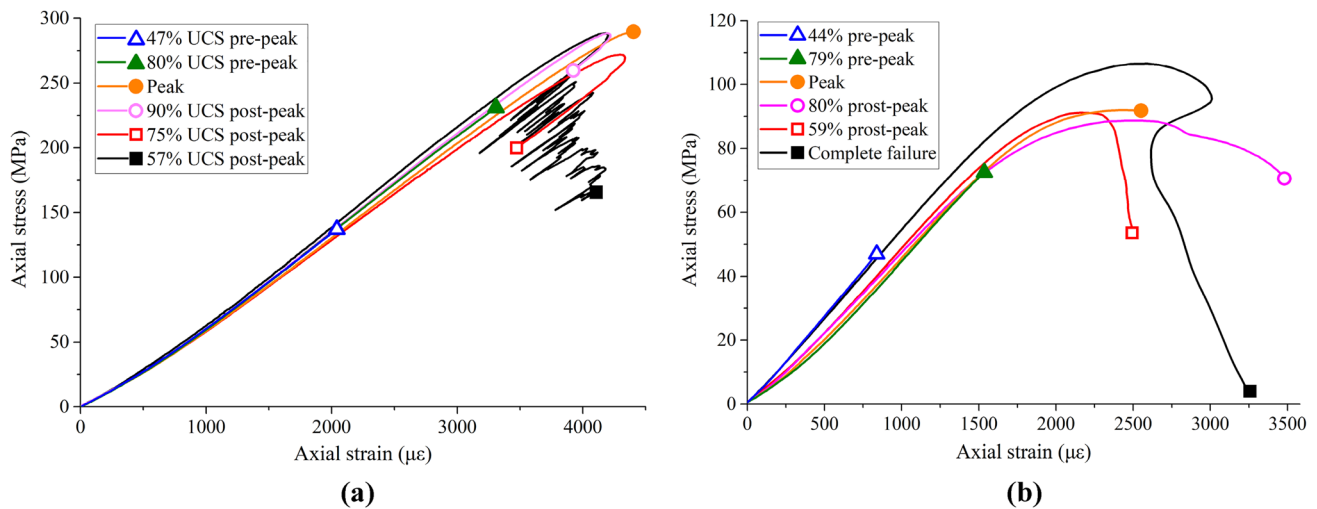


**Fig. 6** Stress–strain curves of the **a** granite, and **b** marble specimens

Figure 6 shows the corresponding stress–strain curves for all the specimens. The failure modes of the granite and marble specimens were different, with the granite exhibiting splitting fractures parallel with the loading direction, while the marble tending to undergo shear failure. It was noted that the curves of the granite specimens overlapped very well over the entire loading period (Fig. 6a). The curves of the marble specimens overlapped well in the pre-peak stage, but spread out quite a lot in the post-peak stage (Fig. 6b).

### 2.3 Thin Section Sampling

Two thin sections, one parallel with and the other perpendicular to the loading direction, were cut from each specimen after the uniaxial compression testing (Fig. 2). For the marble specimens, the orientation of the vertical sections was cut perpendicularly to the strike of the macroscopic shear fracture plane. The thin sections were then soaked in an epoxy-dye mixture that a yellow fluorescent dye was added to. The yellow-colored epoxy penetrated into the cracks in the thin sections. After the epoxy had cured, one side of the thin section was glued to a glass slide. The sections were ground away 3–5 mm in thickness and the surface was polished using a fine sander. The final polished thin sections were 30  $\mu\text{m}$  thick, with a roughness of 0.25  $\mu\text{m}$ . The size of each thin section was approximately 30  $\times$  20 mm.

### 2.4 Microscopic Observation and Crack Processing Technique

The microscopic observations were conducted on an Olympus BX51 optical microscope. Under ultraviolet light, the epoxy-filled cracks showed up as bright green (Fig. 7a). The scanned image had a resolution of 72 dpi. After scanning the entire thin section, with the aid of a MATLAB program, the crack networks were binarized based on recognition of the epoxy-dye color and ignoring the background. In the binarization graph (Fig. 7b), the black ribbons represent cracks. Then, the width of each crack was eroded toward its center so that each crack was contracted to a thin trendline. By doing this, the skeletal structure of the crack network was obtained (Fig. 7c). After ignoring the intersection points in the crack network, the crack network was discretized into multiple isolated cracks. The start and end points of each crack were connected to present a linear structure (Fig. 7d). The length of the crack network was calculated from its skeletal structure while the orientation of each crack was determined using the linear frame of the crack network. By laying the crack network over polarizing scanned images, the distribution of the cracks in relation to the mineral grains was made more distinct (Fig. 7e, f). Then, the intergranular and intragranular cracks were distinguished.

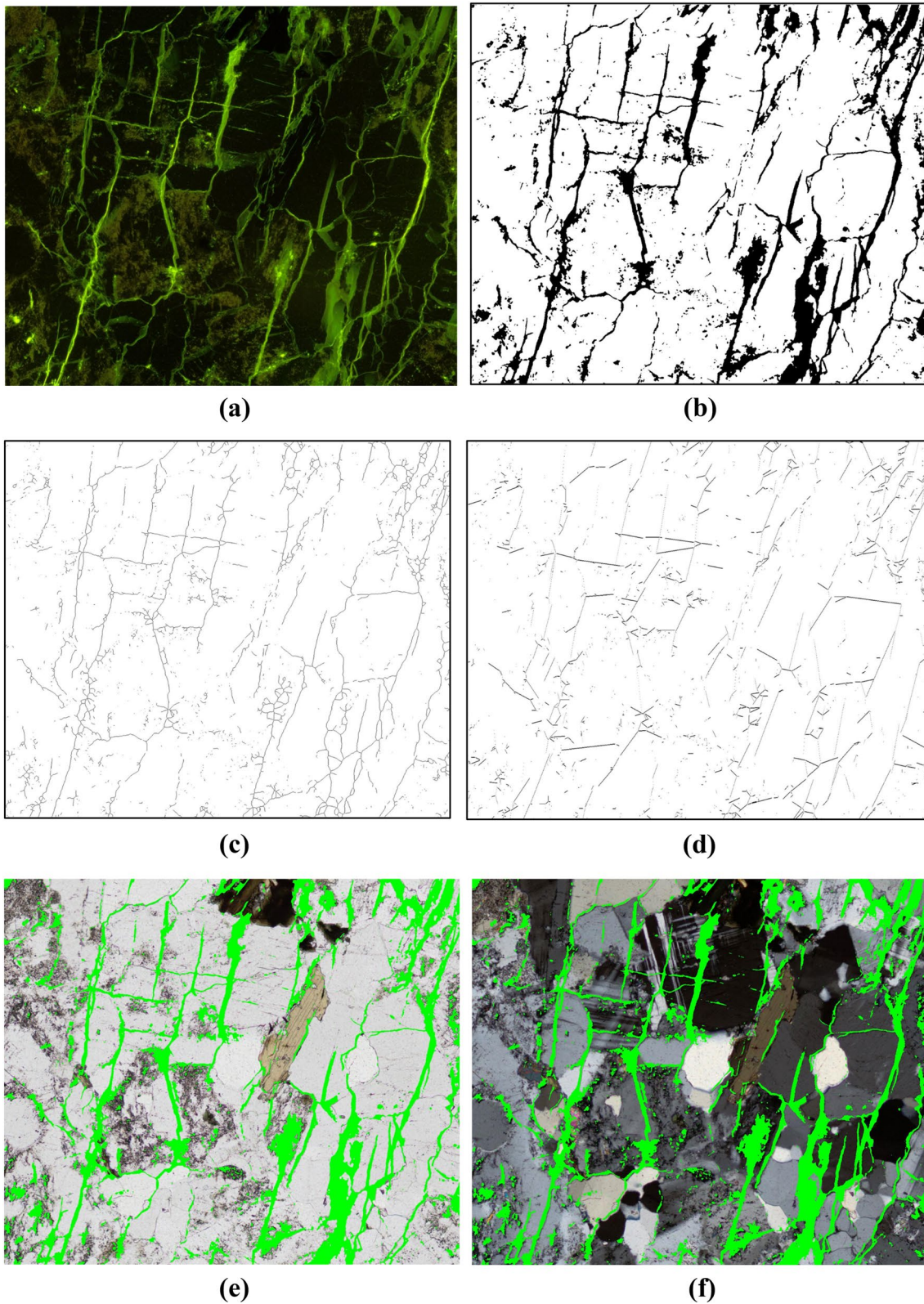


**Fig. 7** Crack network identification: **a** cracks filled with epoxy dye appear bright green under ultraviolet light; **b** crack binarization; **c** crack skeletonization; **d** crack linearization; **e** the crack network on a

plane-polarized image of mineral grains; and **f** the crack network on a cross-polarized image of mineral grains. Note: mineral colors may be different between plane-polarized and cross-polarized images

### 3 Experimental Results and Analysis

The granite specimens loaded to 47% UCS and 80% UCS pre-peak appeared to be relatively undamaged. Hardly any fractures were visible on the surface. When being loaded to peak stress, some linear white patches, parallel with the loading direction, started to appear in the middle of the specimens. These were fractures. With an increase in load, the fracture zone expanded and bulged, and the number and the area of white linear patches increased. At the stress level of 57% UCS post-peak, these patches connected and spread to cover a larger area. These linear fractures showed extensional deformation. Flaky debris could be seen in the fractured area. After peak stress, there were some crisp

cracking sounds. The specimen failed in splitting, accompanied with some mineral powder. In general, however, the fracture surfaces were relatively fresh and clean, showing the original color of the granite grains.

As in the granite, fractures did not appear on the surface of the marble specimens until peak stress. But, differently, the fracture zone in the marble was characterized by the development of diffuse white patches of a wider areal extent. The fracture zone was a band running through the entire specimen at about 30° to the loading direction. It did not bulge significantly. The marble specimens often failed suddenly, accompanied by a large amount of powder. The sides of the fracture zone slipped. The fracture surfaces were covered with abundant lusterless mineral powders. The marble showed obvious shear failure characteristics.

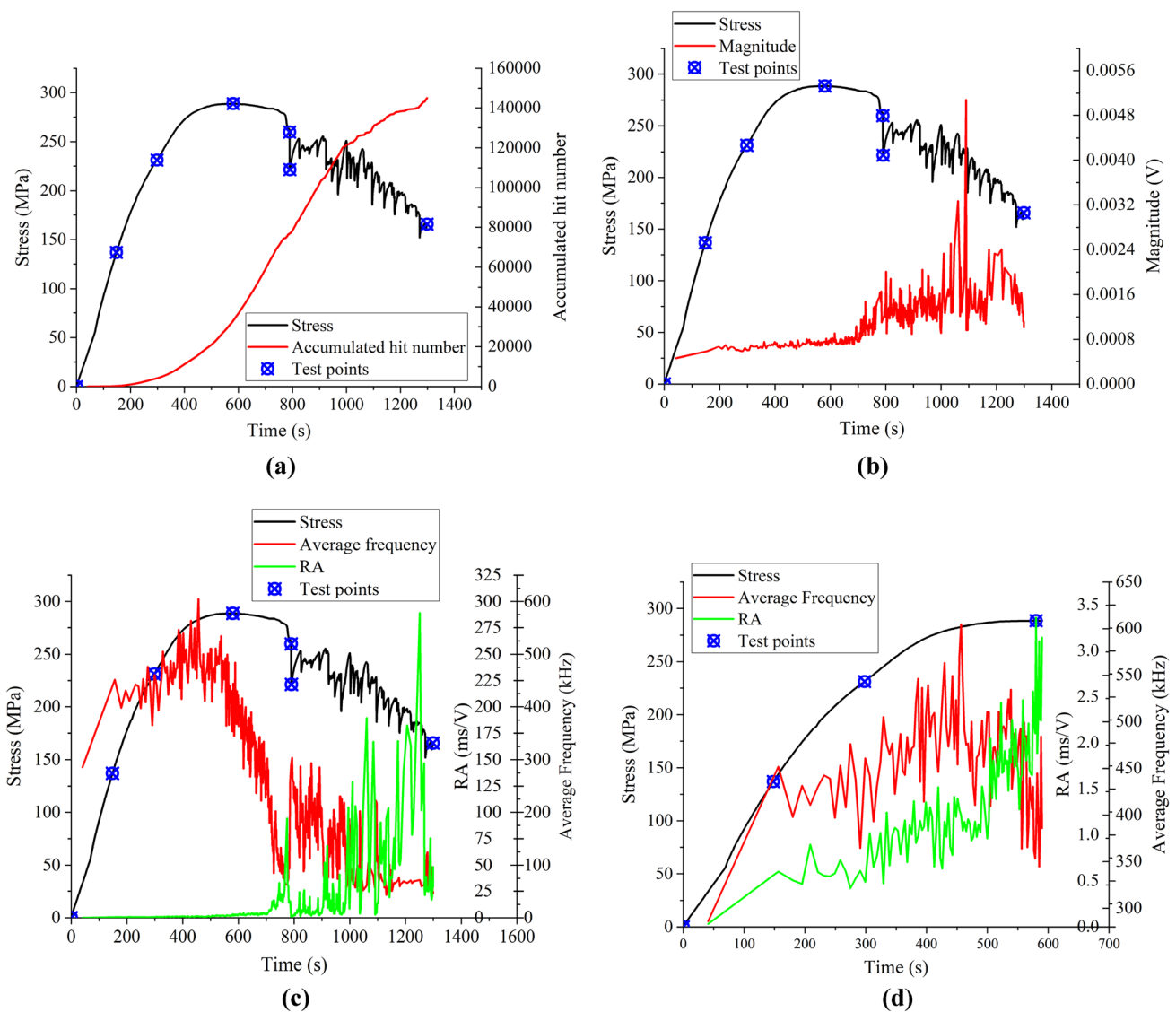


**Fig. 8** Stress and AE records versus time during the granite testing: **a** stress and accumulated AE hits; **b** stress and AE-magnitude hits; **c** stress, average AE frequency and RA; and **d** stress, average AE frequency and RA in the pre-peak stage



The uniaxial compression strength obtained in the tests was, on average, 288.93 MPa for the granite and 95.52 MPa for the marble. The average Young's moduli and Poisson's ratios were 74.88 GPa and 0.29 for the granite, and 53.91 GPa and 0.33 for the marble, respectively.

### 3.1 Acoustic Characteristics During Rock Failure

AE activities reflect the evolution of damage and fracturing in rocks (Luo et al. 2020). They are directly associated with microscopic cracking in the rock material (Lockner et al. 1991). AE is a kind of non-stationary signal that is commonly analyzed using fast Fourier transformation (FFT). Consequently, the magnitude of AEs can be acquired by FFT from recorded AE waveforms. It has been found that the AE signals of extensional fracture have a relatively high average frequency and a low ratio of the rising time to the AE amplitude (RA), while for shear fracture, the average frequency is low and the RA is high (Ohno and Ohtsu 2010). In this study, AE technique was used as an auxiliary means to assist in the microscopic observations to understand the physics of rock burst in the Class II Kuru granite and the reasons for the difference in the fracturing features in the two rock types. Based on the number and frequency domain parameters of AE signals, we quantitatively evaluated the fracturing processes of the rocks. These AE parameters are related to the number, magnitude, type and pattern of the microcracks. Accordingly, the use of AE technique is helpful to understand the microscopic observations. In the meantime, with the help of AE monitoring, the specimen can be loaded under control to a desired level suitable for observation. Figure 8 presents the variations in four AE parameters—the accumulated AE hits, the magnitude, the average frequency and the RA—that occur during the compression testing of a granite specimen. The deformation and damage process can be divided into five stages—crack closure, elastic deformation, stable crack growth, unstable crack growth and post-peak failure.

There were several discrete AE hits during the crack closure and elastic deformation stages at approximately below 40% UCS (Fig. 8a). These discrete AE hits may be related to microcrack compaction and adjustment of the loading and seating. The deformation of the rock was dominantly elastic. After entering the crack initiation and stable growth stage (approximately 40–85% UCS), the number of AE hits gradually increased with an increase in stress (Fig. 8a), indicating a moderate microcracking process. The AE hits exhibited small or moderate magnitudes in this stage (Fig. 8b). The average frequency of the AE signals was high and the RA was very low (Fig. 8c), indicating that extensional fractures dominated in this stage. Both slightly increased with increased stress, as shown by the magnified curves in

Fig. 8d. With an increase in stress, the existing microcracks grew in a stable way and, also, new cracks were created, resulting in a nonlinear stress–strain behavior.

During the unstable crack propagation stage (approximately above 85% UCS), the number of AE hits increased significantly (Fig. 8a). The cracks propagated in an uncontrolled way, emitting a high amount of AEs. A decrease in the average frequency and an increase in the RA implied that more fractures became shear fractures in that stage (Fig. 8d). The magnitude of the AE hits slightly increased as well (Fig. 8b). The shear fractures with higher magnitudes released more energy.

After entering the post-peak stage, the number of AE hits abruptly increased, accounting for two-thirds of the total AE hits (Fig. 8a). At approximately 780 s, the average AE frequency dropped significantly, but the RA jumped markedly (Fig. 8c). At that point, a macroscopic shear fracture must have occurred, resulting in a drop in stress, as shown in Fig. 8a. After that, the average frequency increased and the RA decreased, implying that extensional fracturing became dominant again. Each abrupt drop in the average AE frequency and jump in the RA corresponded to a relatively large-scale shear fracture in the rock. It can be seen in Fig. 8c that such drops and jumps occurred several times in the post-peak stage. This means that the extensional and shear fracturing were intermittent and alternating in the post-peak stage. This agrees with the observations of other studies (Conrad and Friedman 1976; Moore and Lockner 1995).

In general, shear fracturing starts to appear in the unstable crack growth stage. Shear fractures bring about AE hits with high RAs, low average frequencies and high magnitudes. They also release more AE energy than extensional fractures. An abrupt jump in the RA and a sudden drop in the average frequency are indicators of shear fracturing.

Based on the AE characteristics, the failure process of the marble can be divided into three stages—pre-peak linear, pre-peak nonlinear and post-peak (Moradian et al. 2010). In the pre-peak linear stage (approximately below 45% UCS), the original flaws in the rock were gradually closed under compression. A few AE signals were observed in this stage (Fig. 9a), so little damage occurred. In the pre-peak nonlinear period (approximately above 45% UCS), the AE hits increased gradually (Fig. 9a). This AE signal was associated with the initiation of new cracks and the stable propagation of new cracks. The AE hits had small magnitudes, high average frequencies and low RAs, indicating that the cracking was dominantly extensional in this stage (Fig. 9b, d). After reaching peak stress, the number of AE hits began to increase dramatically up to final failure (Fig. 9a). The rate of the AE hits increased markedly prior to final failure. The AE hits in the post-peak stage accounted for 80% of the total hits. In this stage, the average AE frequency decreased and the RA increased,

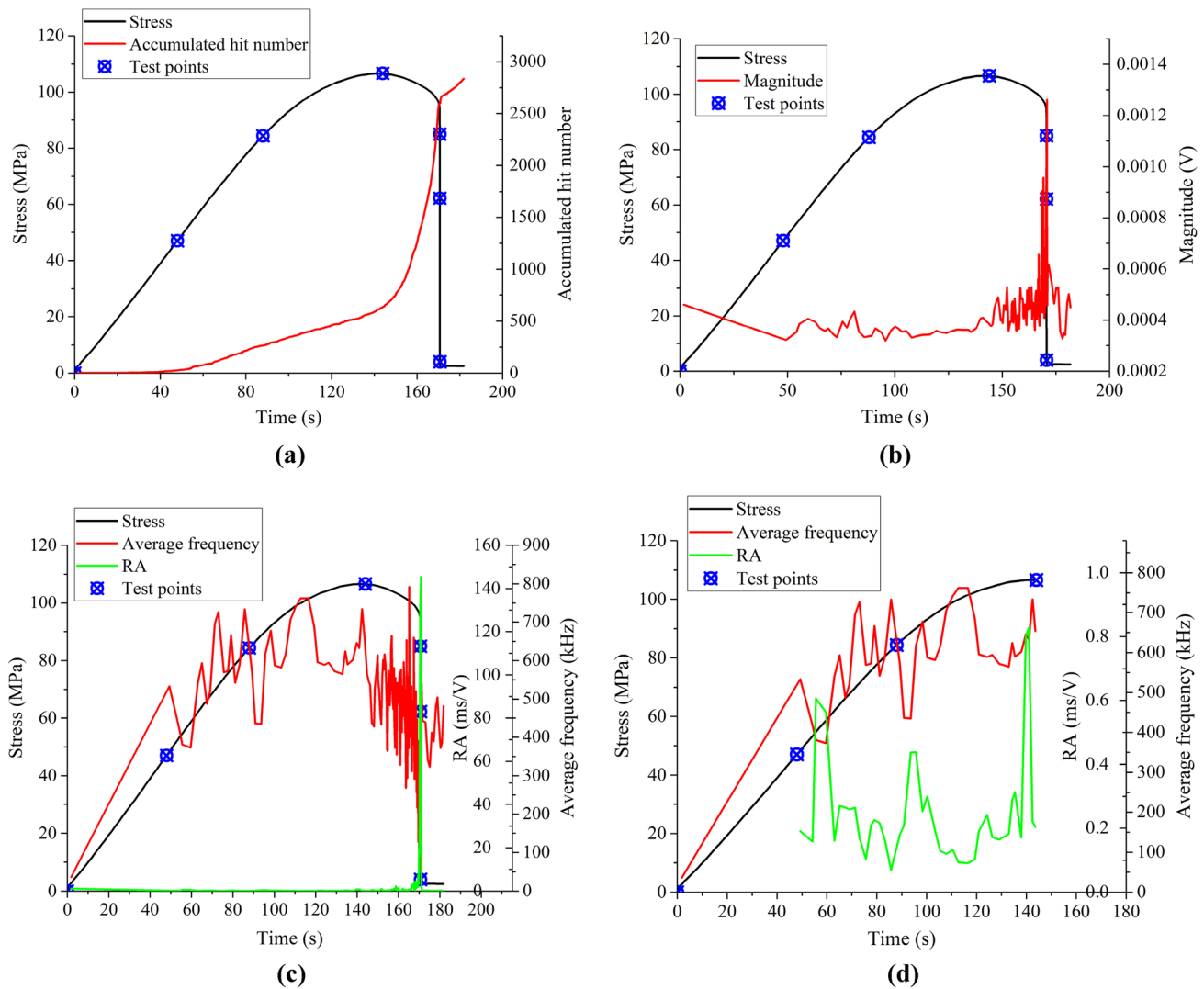


**Fig. 9** Stress and AE records versus time during the marble testing: **a** stress and accumulated AE hits; **b** stress and AE-magnitude hits; **c** stress, average AE frequency and RA; and **d** stress, average AE frequency and RA in the pre-peak stage

indicating that shear fracturing became dominant (Fig. 9c). The sharp increase in AE magnitude meant a large amount of energy was released (Fig. 9b).

The final brittle shear failure mode of the marble was associated with the process of energy accumulation in the pre-peak stage and the sudden energy release in the post-peak stage. The failure mode is defined as brittle when the AE energy is suddenly released in the post-peak stage; otherwise, it is plastic (Guo and Dong 2019). As shown in Fig. 9b, the stress dropped suddenly prior to final failure, and AE hits with high magnitudes were emitted suddenly. Thus, brittle shear failure occurred in the Fauske marble.

Based on their AE characteristics, the Kuru granite and Fauske marble had different failure and energy release processes. Unstable crack propagation started at pre-peak 85% UCS in the granite, while it started in the post-peak stage

in the marble. Unstable crack propagation was related to shear fracture. During stressing of the granite and marble specimens, the initial fractures were extensional. The granite finally failed in splitting, even though shear fracturing was certainly involved in the process, while the marble finally failed by shearing due to the dominant shear fracturing in the specimen. The majority of the AE hits were emitted when the stress was above 80% UCS in the pre-peak stage and in the post-peak stage in the granite, while the majority of the AE hits were emitted upon shear failure in the marble.

**Fig. 10** Photomicrographs of fracture networks in thin sections cut from the granite specimens loaded to the level of: **a** 0; **b** 47% UCS pre-peak; **c** 80% UCS pre-peak; **d** 100% UCS; **e** 90% UCS post-peak; **f** 75% UCS post-peak; and **g** 57% UCS post-peak, respectively. Note that S|| refers to the vertical thin section that is parallel with the loading direction and S⊥ to the horizontal thin section that is perpendicular to the loading direction, and I refers to the intergranular cracks and T to the intragranular cracks

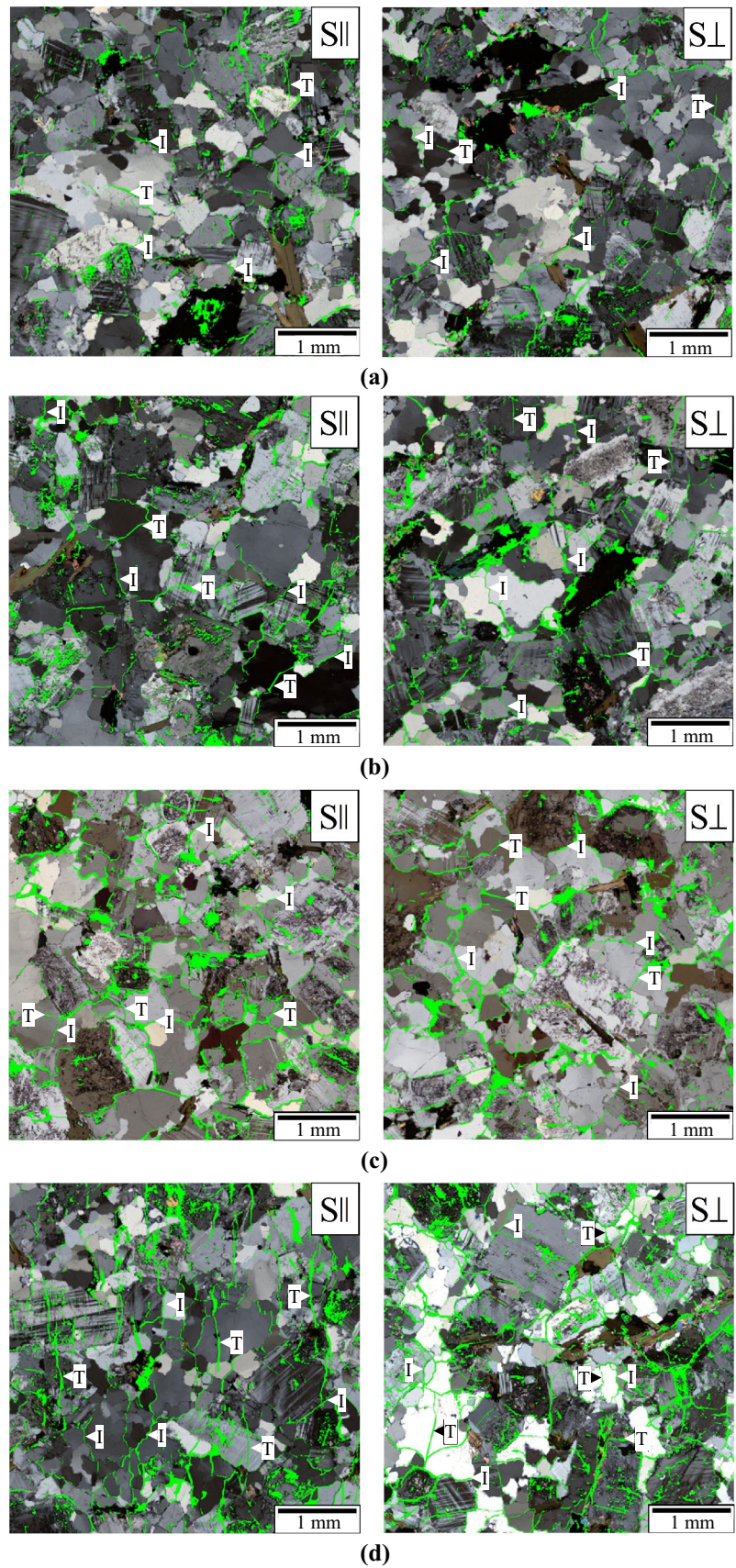
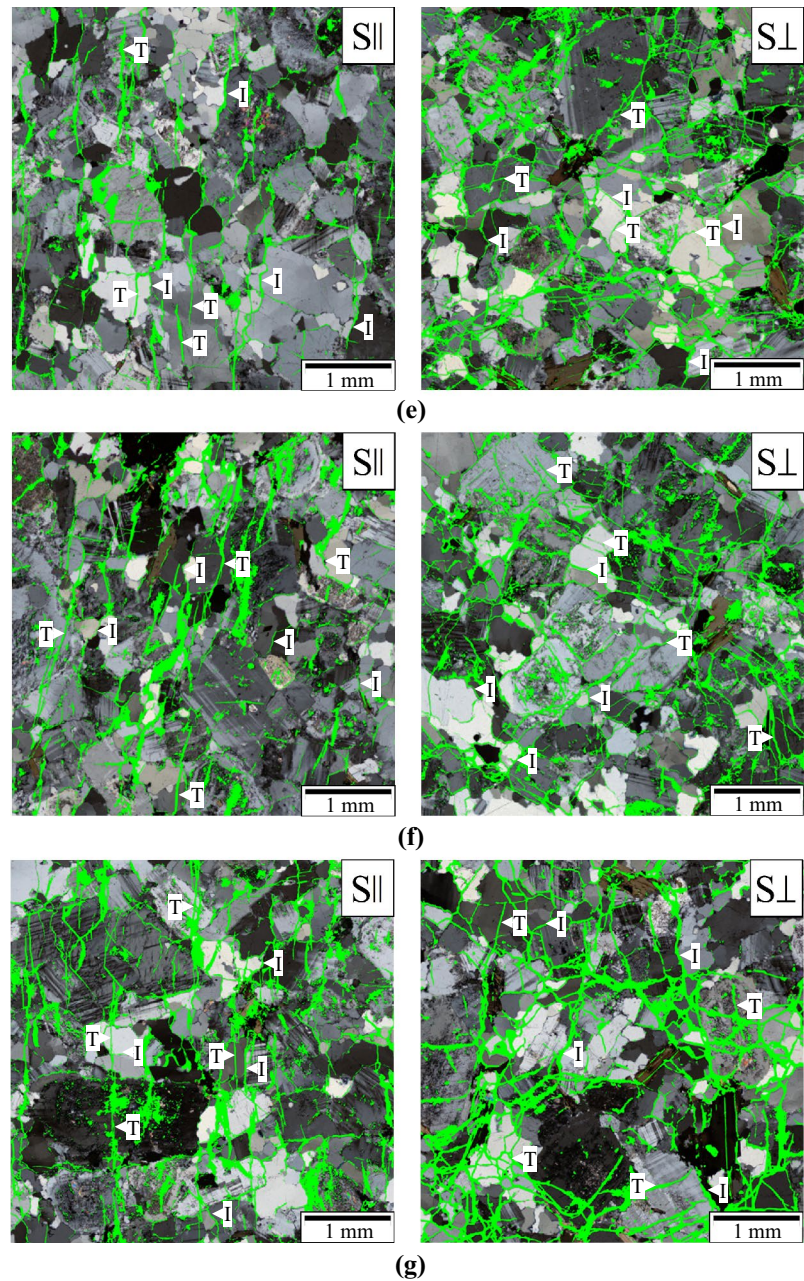


Fig. 10 (continued)



### 3.2 Microscopic Crack Development During Failure

#### 3.2.1 Microscopic Crack Development in the Granite

The AE results suggest that cracks were initiated and grew stably as the applied stress reached approximately 40% UCS in the granite. The fracturing process in the rock was examined microscopically using the thin sections that were cut parallel (labeled  $\parallel$ ) and perpendicular (labeled  $\perp$ ) to the loading direction. For comparison, the initial cracks in an unloaded specimen were also microscopically observed. Figure 10 shows the fracture networks in the granite specimens that were exposed on planes parallel and

perpendicular to the loading direction at different stress levels covering the entire loading period. The pictures in Fig. 10 were only enlarged small portions of the entire fracture network images to show the crack distributions more clearly.

The original flaws in the unloaded granite specimen are shown in Fig. 10a. The original cracks are generally randomly distributed in the vertical ( $S\parallel$ ) and horizontal ( $S\perp$ ) thin sections. The identical initial crack distributions in both directions indicate that the granite is quite homogeneous. At the stress level of 47% UCS pre-peak, the cracks had grown and opened somewhat, but the crack growth was almost identical in both the vertical and horizontal

**Fig. 11** Photomicrographs of fracture networks on thin sections cut from the marble specimens loaded to the level of: **a** 0; **b** 44% UCS pre-peak; **c** 79% UCS pre-peak; **d** 100% UCS; **e** 80% UCS post-peak; **f** 59% UCS post-peak; and **g** 0 post-peak, respectively

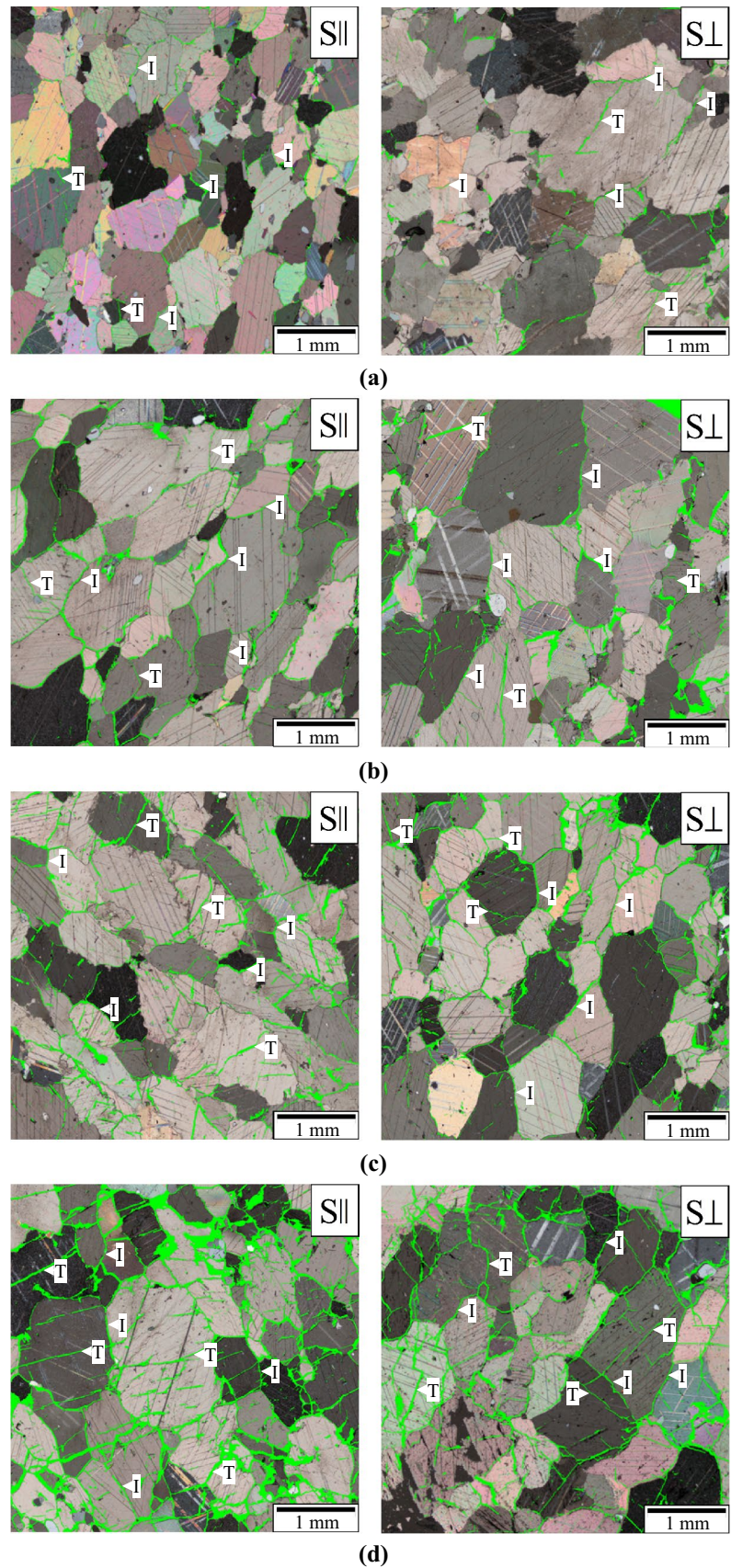
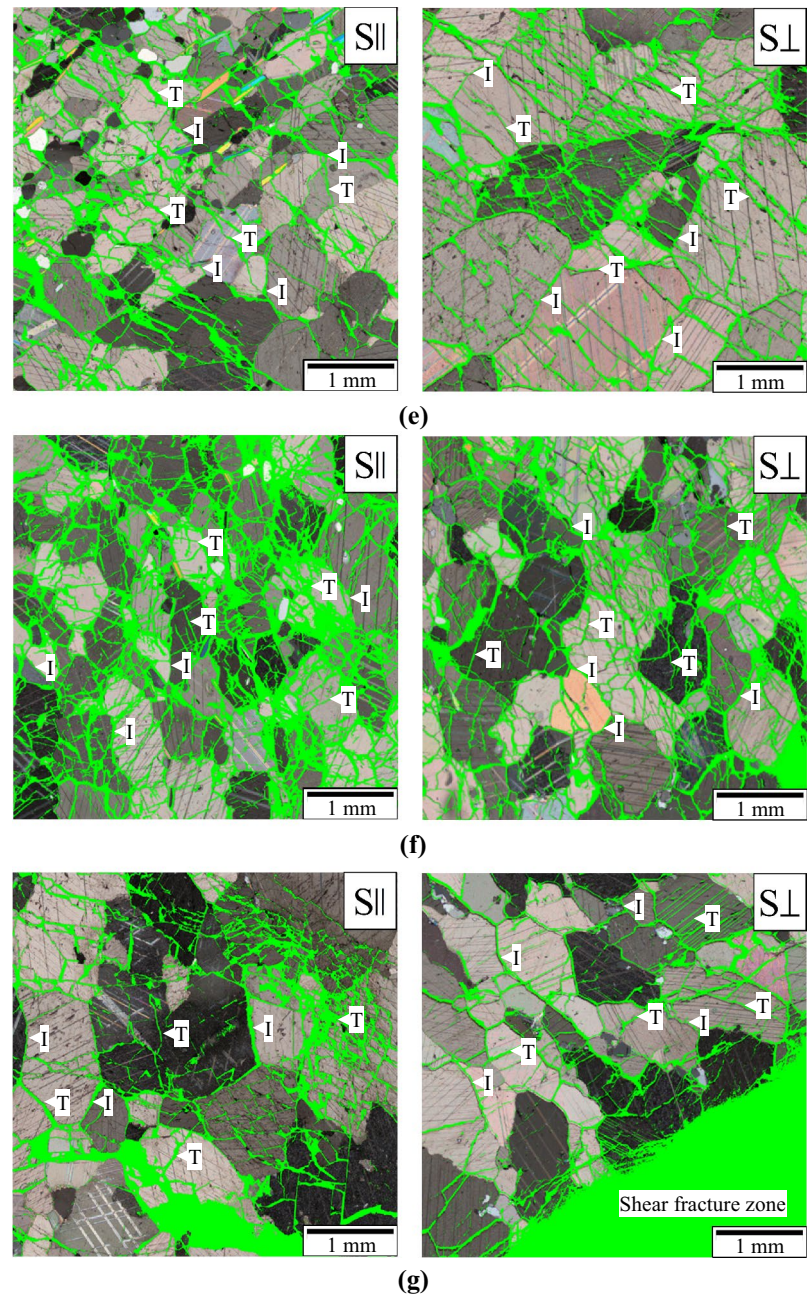


Fig. 11 (continued)



directions, as shown in Fig. 10b. A small number of intragranular cracks had initiated, but intergranular cracks were still dominant up to this stage. At 80% UCS pre-peak, intergranular cracks continued to develop and connect to each other (Fig. 10c). The cracks were markedly widened, with the maximum crack width being around  $12\ \mu\text{m}$ . The crack density was slightly higher in the vertical section than in the horizontal section, indicating that the cracks were already inclined to grow in the vertical direction at 80% UCS pre-peak. At peak stress, the crack growth was strongly anisotropic in the vertical section, but not in the horizontal section (Fig. 10d). The cracks

grew significantly in the vertical direction, and numerous cracks propagated intragranularly. It was observed that some linear white patches, parallel with the loading direction, appeared on the cylindrical surface of the specimen at a level close to peak stress during the test. It seems that axial splitting cracks (i.e., cracks growing in the direction of  $\sigma_1$ ) started to become dominant approximately at peak stress. After the stress passed the peak value, the number of both intergranular and intragranular cracks increased dramatically, and all the cracks extended considerably (Fig. 10e–g). When the stress dropped from 90% UCS (Fig. 10e) to 75% UCS (Fig. 10f) and then to 57% UCS

(Fig. 10e) in the post-peak stage, it appears that the number of fractures remained approximately the same or only increased slightly, but the widths of the fractures increased abruptly with the stress dropped. The marked widening of the fractures led to bulging of the specimen and white patches on the cylindrical surface. The axial propagation fractures finally split the rock material into flakes or splinters. Splitting fractures dominated the failure process of the specimen. The elastic strain energy stored in some of the flakes and debris was finally released, leading to rock ejection.

### 3.2.2 Microscopic Crack Development in the Marble

The AE results indicate that cracks were initiated and grew stably after the applied stress reached approximately 45% of the peak stress in the marble, while the cracks started to propagate unstably as soon as the load crossed peak stress. For the marble, the specimens loaded up to 44% UCS pre-peak, 79% UCS pre-peak, peak value, 80% UCS post-peak, 59% UCS post-peak and complete failure, and one unloaded specimen were microscopically observed in directions parallel and perpendicular to the loading direction. These results are illustrated in Fig. 11. The pictures in Fig. 11 were also only enlarged small portions of the entire fracture network images to show the crack distributions more clearly.

The original microcracks in the marble are shown in Fig. 11a. These cracks looked similar in both the vertical and horizontal thin sections. The majority of the cracks were intergranular along the boundaries of the mineral grains, with a few intragranular cracks within the mineral grains.

At the stress level of 45% UCS pre-peak, the intergranular cracks both extended and widened, and a few intragranular cracks also extended (Fig. 11b). When the stress was increased to 79% UCS pre-peak, the sample underwent non-linear deformation, and the intergranular cracks propagated further and connected to each other, and also a good number of intragranular cracks were initiated (Fig. 11c). The long and connected cracks in the vertical section were oriented in directions not parallel with, but deviated from, the vertical loading direction. The cracks did not widen much during the period of stress increase from 44% to 79% UCS in the pre-peak stage. At peak stress, the intergranular cracks further widened and propagated, and a considerable number of intragranular cracks were initiated and grew along the twin cleavages in the minerals (Fig. 11d). This type of intragranular cracking was also observed by Cheng et al. (2016). The cracks showed a certain preferred direction. After passing peak stress, dense intragranular cracks were quickly initiated, propagating extensively (Fig. 11e). The cracks connected with each other, forming long and open fractures that were oriented in a preferred direction. The dominating fractures occurred in a direction approximately 40° from the loading direction in the vertical thin section, as shown in Fig. 11e. Figure 11f shows the fracture networks in the vertical and horizontal thin sections when the stress dropped to 59% UCS in the post-peak stage. The fractures coalesced, and a shear fracture zone was formed. The cracks in the shear fracture zone propagated in all directions before the zone was finally fully formed. In the end, the marble specimen failed by shearing along a fracture zone. Numerous mineral particles were crushed, and fine mineral powders

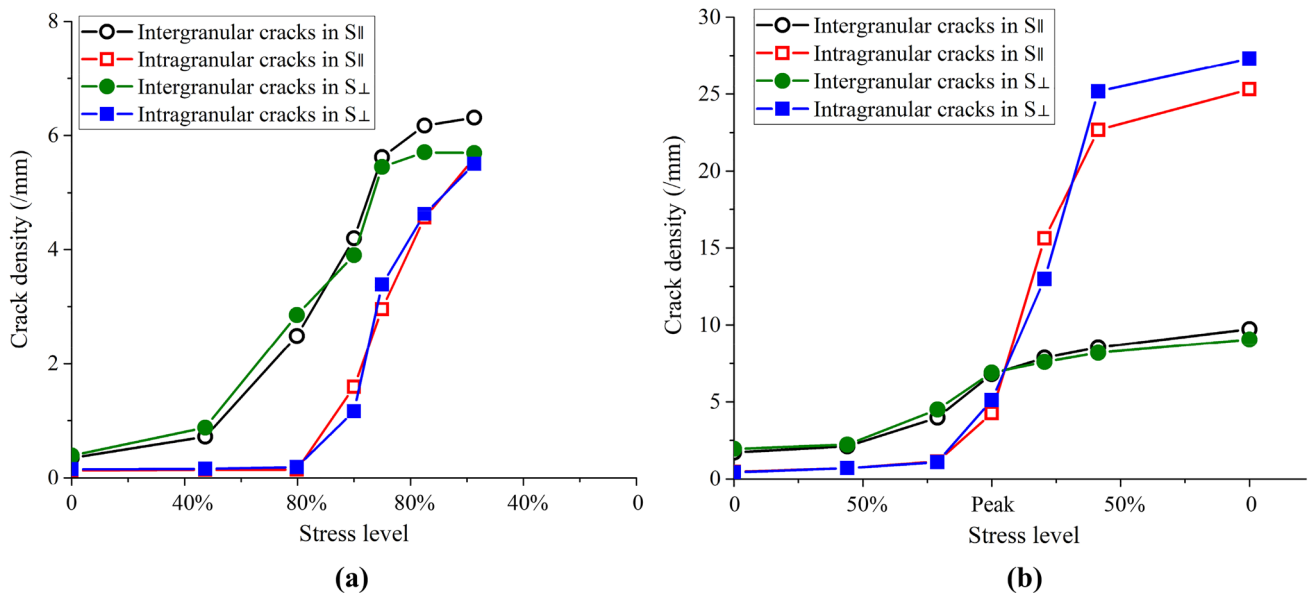


Fig. 12 Variation in crack densities versus stress level in vertical (S<sub>||</sub>) and horizontal (S<sub>⊥</sub>) sections in the a granite, and b marble specimens

covered the surface of the shear fracture plane. Figure 11g shows the fractures next to the main shear fracture plane that is marked by the massive green coloration from the epoxy dye in the images.

### 3.3 Geometric Analysis of the Crack Network

After the crack networks colored by epoxy dye in the thin sections were binarized, the skeletal structure and linear frame of the crack network were outlined, as shown in Fig. 7. The crack network can be quantitatively described by the crack density, the average opening width of the cracks and an orientation factor for the crack inclinations. The crack density is defined as the average length of all cracks in the area of the thin section. It is expressed as (Zhou et al. 2012):

$$D = \frac{1}{A} \sum_{i=1}^n l_i \quad (1)$$

where  $D$  is the crack density in /mm,  $l_i$  is the length of the  $i$ th crack ( $i = 1, \dots, n$ ) and  $A$  is the area of the thin section. This definition of the crack density has been commonly adopted in the stereological study of crack geometry (Litorowicz 2006; Samaha and Hover 1992). The length of the crack network was determined by its skeletal structure. The densities of the intergranular and intragranular cracks in the vertical and horizontal thin sections of the granite and marble were calculated based on the scanned data in the entire thin sections. The variation in crack density versus the applied stress are shown in Fig. 12.

The diagrams in Fig. 12 show that the densities of the intragranular cracks are approximately zero in the unloaded specimens (i.e., at zero stress in the diagrams). In the unloaded specimens, the crack densities in the two orthogonal directions are approximately identical, which quantitatively indicates that both the granite and marble are quite homogeneous, as shown in Fig. 12. For the granite (Fig. 12a), the density of the intergranular cracks increased slightly from 0.37/mm to approximately 0.8/mm when the stress was increased from zero to 47% UCS. The crack density continued to increase to 2.67/mm when the stress was further increased to 80% UCS in the pre-peak stage. In this stage, however, the density of the intragranular cracks remained at the original level of about 0.15/mm. Following that, the density of the intragranular cracks abruptly increased and remained on the increase through the rest of the pre-peak loading stage and in the post-peak stage. The density of the intergranular cracks remained on the increase, too, although the increasing rate was retarded after peak stress. At the stress level of 57% UCS in the post-peak stage, the densities of the intergranular and intragranular cracks were at similar levels. It can be seen in the diagrams that the densities of the intergranular cracks are approximately identical in both the vertical and horizontal directions. This is also the same tendency for the intragranular cracks. The crack densities in the two orthogonal directions should be identical because the granite is homogeneous. The small differences in crack density in the two directions may have been caused by the calculation method.

For the marble specimens (Fig. 12b), the densities of the intergranular and intragranular cracks vary in similar

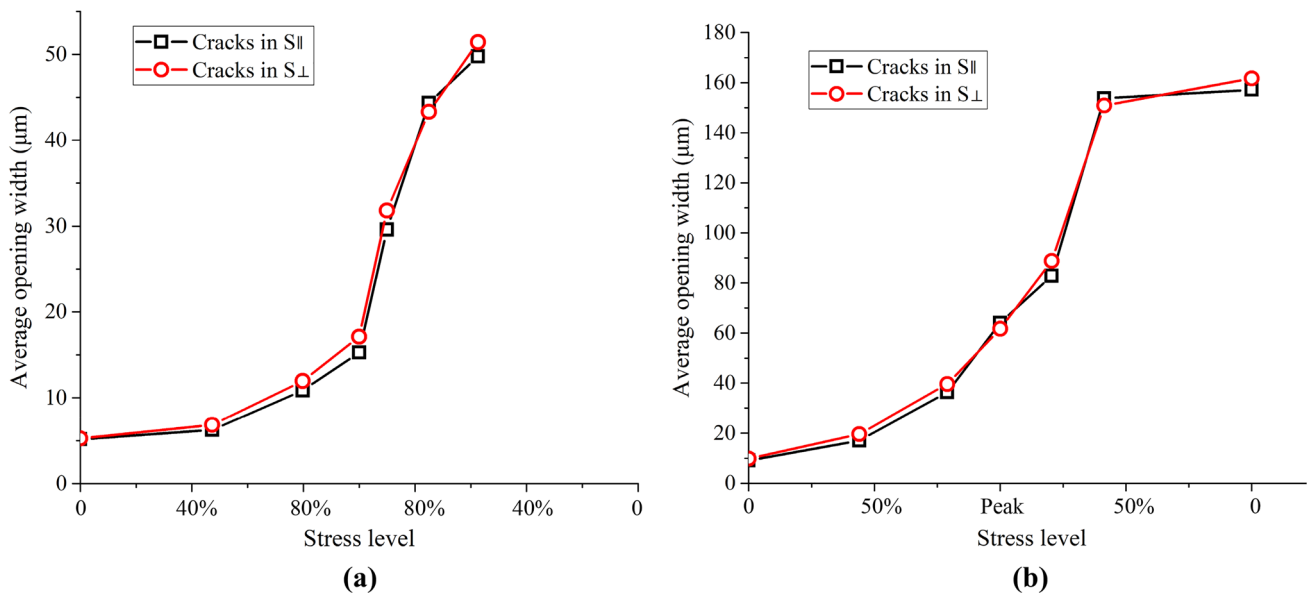


**Fig. 13** Variation in average crack opening widths versus stress level in vertical (S<sub>||</sub>) and horizontal (S<sub>⊥</sub>) sections in the **a** granite, and **b** marble specimens



tendencies with the applied stress in the two orthogonal thin sections. The densities of the intergranular cracks are approximately identical in both the vertical and horizontal directions. The intragranular cracks also show this characteristic. The densities of the intergranular cracks in the two orthogonal directions started to increase identically at the stress level of 44% UCS in the pre-peak stage, and remained on the increase through the entire loading and unloading periods afterward. The increasing rate in crack density also became retarded after peak stress. The densities of the intragranular cracks in the two orthogonal directions remained approximately the same as in the unloaded specimen until the applied stress was at the level of 79% UCS in the pre-peak stage. Following that, the crack densities

abruptly increased with applied stress. The increasing rates became retarded after the stress dropped below the level of 59% UCS in the post-peak stage. It should be noted that the densities of the intragranular cracks exceeded the densities of the intergranular cracks after the stress passed the peak value. This implies that intragranular fracturing dominated in the post-peak stage.

The average opening width ( $W$ ) of all the cracks in the specimen is defined as:

$$W = \frac{\sum_{i=1}^n A_i}{\sum_{i=1}^n l_i} \tag{2}$$

where  $A_i$  ( $i=1, \dots, n$ ) is the opening area of the  $i$ th crack. The calculated average opening widths of the cracks in the vertical and horizontal thin sections of the granite and marble are presented in Fig. 13.

The curves in Fig. 13 indicate that the crack opening width increased slowly in the stages where intergranular cracks dominated, but the crack opening became marked after the intragranular cracks flourished. During crack propagation, the fracture surfaces slipped, and the surface asperities dislocated to widen the apertures between the fracture surfaces. The average crack opening width in the marble was much bigger than that in the granite. This might be attributable to the numerous intragranular cracks in the marble. In the granite, the crack opening remained on the increase until flakey debris occurred, while in the marble, after the stress dropped to 59% UCS in the post-peak stage, the crack opening stopped, indicating that the failure was dominated by crack coalescence afterward.

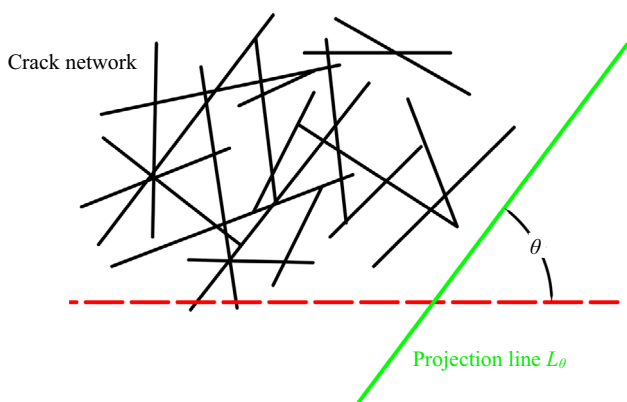


Fig. 14 Sketch illustrating calculation of the total projection length  $\zeta(\theta)$  in the orientation  $\theta$

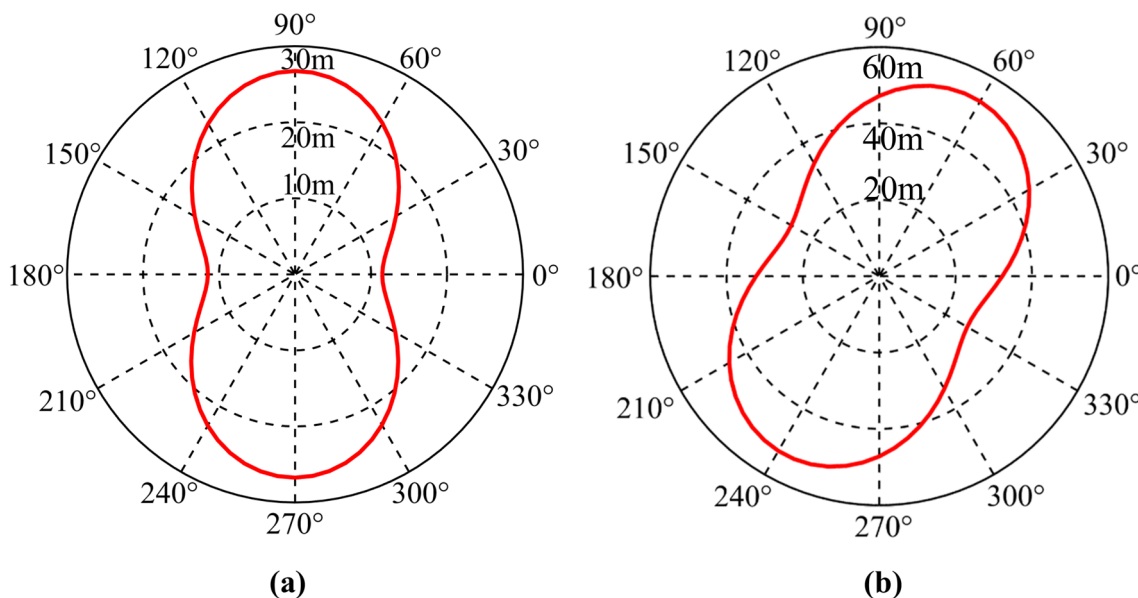
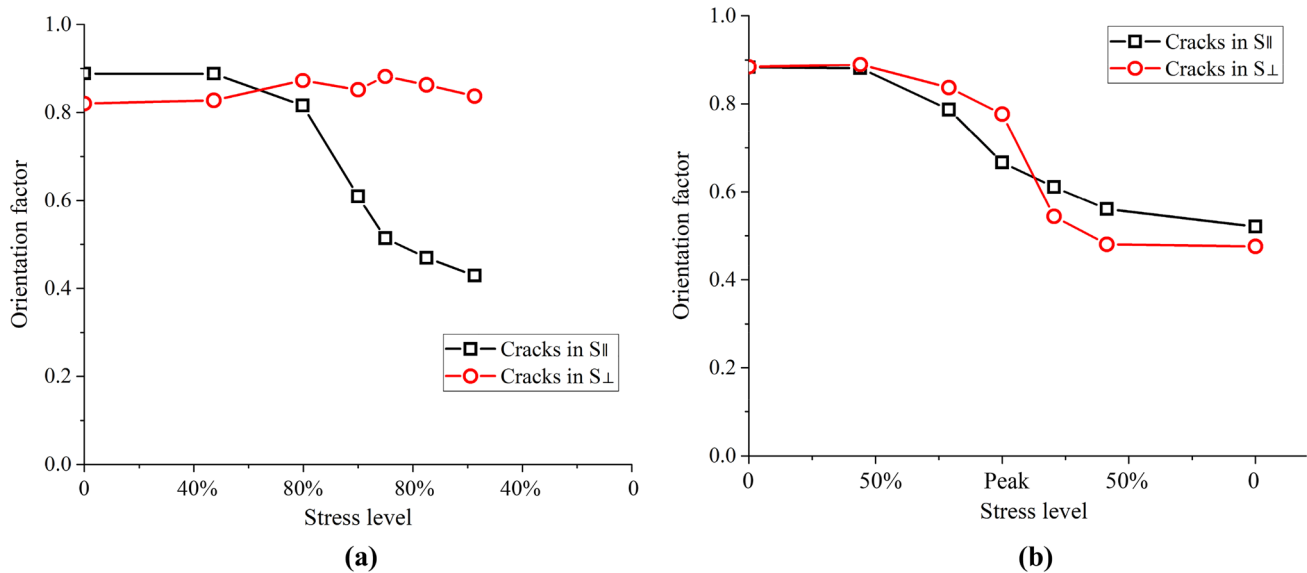


Fig. 15 Projection lengths  $\zeta(\theta)$  of the crack cluster in the vertical thin section SII of the **a** granite specimen loaded to 57% UCS in the post-peak stage, and **b** marble specimen loaded to final failure



**Fig. 16** Variation in orientation factors of the crack cluster in the vertical ( $S_{||}$ ) and horizontal ( $S_{\perp}$ ) thin sections of the **a** granite specimens, and **b** marble specimens loaded to different stress levels

The dominant propagation orientation of a crack network in a specimen can be estimated using the following method. Consider a cluster of  $n$  randomly distributed cracks, as illustrated in Fig. 14. The length of the  $i$ th crack is projected onto the projection line,  $L_{\theta}$ , with an angle,  $\theta$ , to the horizontal line. The projection lengths of the crack cluster are summed, and the total projection length of the cracks in the orientation of  $\theta$  is denoted as  $\zeta(\theta)$ . The projection lengths of the crack cluster in different orientations are obtained by varying the projection angle,  $\theta$ , in the range  $0$ – $360^{\circ}$ . The projection lengths of the cracks were calculated in this way for the granite specimen loaded to 57% UCS in the post-peak stage and for the marble specimen loaded up to complete failure. The calculated results for the two specimens are presented in the polar diagrams in Fig. 15. The radii of the circles in the diagram represent the total projection crack lengths, and the angle is the orientation that the crack lengths are projected to. The orientation factor,  $\omega$ , of the crack propagation is defined as (Ammouche et al. 2001):

$$\omega = \zeta(\theta)_{\min} / \zeta(\theta)_{\max} \quad (3)$$

where  $\omega = 1$  means that all cracks propagate identically in all directions and  $\omega = 0$  means that all cracks propagate in one direction. In general, the dominant crack-propagating orientation is the one that the maximum projection length  $\zeta(\theta)_{\max}$  is oriented in. The value of factor  $\omega$  depicts the isotropy in the crack propagation in the specimen. Figure 16 provides variations of the orientation factor versus the applied stress in the granite and marble specimens.

For the granite, the orientation factor,  $\omega$ , was between 0.8 and 0.9 from the start of the loading up to the stress level of 80% UCS in the pre-peak stage in both the vertical and horizontal thin sections, implying that the crack propagation was identical in all directions for that loading period. After the stress was above 80% UCS, the orientation factor in the vertical thin section decreased, dropping to approximately 0.4 at the stress of 57% UCS in the post-peak stage (Fig. 16a). The orientations of the maximum total projection lengths in the specimens changed to the vertical direction. This indicates that crack propagation gradually became dominant in the loading direction after the applied stress was above 80% UCS. The orientation factor in the horizontal thin section, however, remained unchanged at a level of 0.8–0.9 up to the end of the test, indicating that the crack propagation was identical in all directions in the orientation perpendicular to the loading direction. For the marble, the orientation factor,  $\omega$ , remained unchanged at 0.9 in both thin sections until the stress was increased to 44% UCS in the pre-peak stage (Fig. 16b). After that, it decreased with increasing stress in the pre-peak stage and with the stress drop in the post-peak stage. The orientation factor dropped to approximately 0.45 at the stress of 59% UCS in the post-peak stage, remaining unchanged at that level until the stress dropped to zero. According to the diagram in Fig. 15b, the cracks in the vertical plane preferably propagated in an orientation of about  $27^{\circ}$  to the loading direction. The orientation factor varied similarly in the vertical and horizontal thin sections, implying that the cracks propagated in preferred directions in both the vertical and horizontal planes.

## 4 Discussion

### 4.1 Fracture Characteristics in the Granite

At the microscopic scale, intergranular cracks were initiated and propagated first in the granite. Intergranular cracking dominated the entire process. More and more intragranular cracks nucleated in the mineral grains after the stress went above 80% UCS in the pre-peak stage. The intragranular cracks propagated preferably in the loading direction. The intergranular and intragranular cracks were distributed uniformly, gradually coalescing to form numerous vertical macroscopic fractures that were visible on the cylindrical surface of the specimen in the form of linear white patches. In the final failure stage, the fractures split the specimen into flakes and splinters, accompanied by loud and crisp cracking sounds. The surfaces of the splitting fractures were relatively fresh and clean, implying that the surfaces were barely subjected to shearing damage since they were created.

### 4.2 Fracture Characteristics in the Marble

Similarly to the granite, intergranular cracks were the first to initiate and propagate in the marble. Differently from the fracture development in the granite, however, intragranular cracking became dominant in the post-peak stage in the marble. The numerous intragranular cracks may be attributable to the pre-existence of a number of weak twin cleavages in the calcite grains. The twin cleavages in the direction of the maximum effective shear stress started to slip, followed by slippage in cleavages in other directions. Such cleavage slippage occurred at 10° and 30° to the loading direction, as has previously been found in other studies (Moradian et al. 2010; Ohno and Ohtsu 2010). With an increase in the applied stress, the material between the slipping cleavages was crushed to form shear fractures. The shear fractures were visible as inclined diffuse white patches on the cylindrical surface. In the final failure stage, a major shear fracture zone formed at an angle of about 27° to the loading direction. A significant number of cracks occurred in the areas close to the fracture zone. The shear fracture surfaces were covered in calcite powder.

The primary feature of the failure in the marble is that the number of the spalling grains, the fracturing degree and the crack opening width increase with loading. According to the Mohr–Coulomb failure criterion (Labuz and Zang 2012), the shear stress is related to the apparent friction angle that is affected by the surface roughness (Li et al. 2019). It can be deduced that the broken asperities bear the shear load mainly by sliding friction while the unbroken shear bearing

asperities on the other parts of the fractured zone bear the shear load by static friction. According to the AE data (Fig. 9), the complete shear slippage did not occur before the peak stress. As more and more unbroken asperities were mobilized, the ultimate shear stress was gradually reached. After a great number of asperities in the fractured zone were crushed and ground to powder, the ultimate shear stress was exceeded and shear slippage occurred, releasing a number of AE signals. After that, the fracture surface roughness and the shear stress decreased. As more asperities were crushed, the rock macroscopically failed in shear along the fractured zone. A number of AEs were generated, and a great amount of energy was dissipated in this period.

### 4.3 Intergranular and Intragranular Cracking

Intergranular and intragranular cracks are the two types of cracks that appear in rocks in the process of rock failure. The initial cracks were intergranular in both the brittle granite and the relatively soft marble. Intergranular cracks occur along the mineral grains and in all directions. Intragranular cracks are nucleated later than intergranular cracks (DiGiovanni et al. 2007), and propagate in preferred directions. The intragranular cracks propagated in the loading direction in the granite, but in an inclined orientation to the loading direction in the marble. The appearance of abundant intragranular cracks marks the commencement of unstable fracturing in a rock. At the end, the intergranular and intragranular cracks coalesced to form either vertical fractures that split the brittle granite or macroscopic shear fractures in the soft marble.

Intragranular cracking emits more AEs than intergranular cracking, since the energy release rate of intragranular cracking is usually several times that of intergranular cracking (Abdollahi and Arias 2012; Tatami et al. 1997). The AE signals had relatively small magnitudes when intergranular extensional cracking dominated the damage process at low stress levels, while in the unstable intragranular cracking stage, the magnitudes of the AE signals were significantly higher, as shown in Figs. 8b and 9b. Accordingly, a macroscopic shear fracture that involves dominant intragranular cracking will produce AE events of greater magnitudes than an extensional fracture that involves dominant intergranular cracking. These results agree with certain other experimental results on AE signals (Graham et al. 2010; Kwiatek et al. 2014).

### 4.4 Relationship Between Fracture Characteristics and Burst-Proneness

As mentioned above, the Kuru granite was burst-prone, but the Fauske marble was not. The development processes of the microcracks in the two rocks may be helpful in understanding the mechanics of these differences in burst-proneness. The cracks in the granite dominantly propagated in the

loading direction, and the rock split into flakes and splinters at the end. The fracture surfaces were clean, indicating the fracture was extensional. Both the crack density and average crack opening width were very small compared to those in the marble (Figs. 12, 13). Therefore, a relatively small part of the elastic energy in the rock was dissipated through fracturing in the granite. The remaining part of the elastic energy had to be released in the form of kinetic energy, bringing about rock ejection and rock burst.

In the marble, the cracks propagated in a preferred orientation, inclined toward the loading direction, and the rock finally failed along a number of shear fractures as well as in a wide fracture zone. Both the single shear fractures and the fracture zone were filled with crushed and ground calcite powder. The final crack density in the marble was more than four times that in the granite (Fig. 12), and the final average crack opening width was more than three times that in the granite (Fig. 13). Obviously, a great amount of energy, and probably all the elastic energy in the rock, was dissipated during shear fracturing in the marble. Thus, no elastic energy was left for rock ejection and so no rock burst occurred in the marble.

It seems that rocks subjected to microscopic extensional fracture are burst-prone, while rocks subjected to microscopic shear fracture are not. The intragranular cracking is a key factor in determining whether a rock is burst-prone or not. The significance of the study to rock engineering is that the burst-proneness of the rocks in an excavation project can be assessed based on the amount of the excess energy shown in Fig. 1b.

## 5 Conclusions

A series of laboratory tests were carried out to investigate the microscopic fracturing processes in the Class II Kuru granite and the Class I Fauske marble. The Kuru granite is brittle and burst-prone. The Fauske marble is moderately soft and not burst-prone. The rock specimens were loaded to different stress levels in both pre- and post-peak stages. AE technique was used to monitor the progressive fracturing process. After the load was removed, two thin sections, one parallel and the other perpendicular to the loading direction, were prepared from each specimen. The microcracking networks in the thin sections were observed under an optical microscope. The following conclusions were arrived at based on the AE monitoring and the microscopic observations.

Under uniaxial compression, the dominant microcracking pattern is intergranular and extensional in the Class II and burst-prone Kuru granite, but is intragranular and shear in the Class I and non-burst-prone Fauske marble. The extensional cracks in the Kuru granite propagate in the direction

of the major principal stress,  $\sigma_1$ . The intragranular shear cracks orient in the directions inclined to  $\sigma_1$ .

Microscopic observation of the microcracking in the two types of rocks confirmed that the AE signals of extensional fracturing were of relatively high average frequency and low RA, while the AE signals of shear fracturing were of low average frequency and high RA. The abrupt increase in the number of intragranular cracks was attributed to increases in crack density and crack opening width, and also to the preferred direction of crack propagation.

The intergranular cracks were usually extensional, while the intragranular cracks were in shear. Intragranular cracking releases more AE events than intergranular cracking, and the magnitude of the AE signals from the intragranular cracking was generally greater than the magnitude of the AE signals from intergranular cracking.

Under uniaxial compression, intergranular and extensional cracking dominated the damaging process in the Kuru granite before the stress reached 85% UCS in the pre-peak stage. Following that, more and more intragranular cracks appeared in the rock. In the post-peak stage, the numbers of both intergranular and intragranular cracks increased abruptly, and both propagated in the loading direction. Extensional fractures parallel with the loading direction appeared on the cylindrical surface of the granite specimen in the form of linear white patches prior to final failure. The specimen finally split into thin flakes and splinters. The surfaces of the granite flakes and splinters were fresh and clean.

Under uniaxial compression, only a small number of intergranular cracks existed in the Fauske marble in the pre-peak stage. In the post-peak stage, intergranular cracks only slightly increased, but intragranular cracks become several times more numerous than intergranular cracks. In general, intragranular cracking dominated the damaging process in the marble. The dramatic increase in intragranular cracks was due to slippage along the cleavages in soft mineral grains. Shear fractures inclined toward the loading direction appeared on the cylindrical surface of the marble specimen in the form of diffuse white patches. The surfaces of the shear fractures were covered by finely crushed and ground mineral powder.

Both the crack density and average crack opening width in the granite were very small compared to those in the marble. In the granite, a relatively small part of the elastic energy in the rock was dissipated during fracturing. The remaining part of the elastic energy was released in the form of kinetic energy, bringing about rock ejection and rock burst. The granite therefore has the characteristic of burst-proneness. In the marble, a great amount of energy, and probably all the elastic energy in the rock, was dissipated during shear fracturing. No elastic energy was left for rock ejection and so no rock burst occurred in the marble. The marble does not have the characteristic of burst-proneness.

**Acknowledgements** The authors would like to thank Mr. Gunnar Vistnes for his valuable assistance in the laboratory tests. The authors are also grateful to Mr. Kjetil Eriksen for his valuable assistance in preparing the thin sections. It is acknowledged that the study was supported by the Norwegian University of Science and Technology (NTNU) through the grant SO IV-37/19.

**Funding** Open access funding provided by NTNU Norwegian University of Science and Technology (incl St. Olavs Hospital - Trondheim University Hospital).

**Open Access** This article is licensed under a Creative Commons Attribution 4.0 International License, which permits use, sharing, adaptation, distribution and reproduction in any medium or format, as long as you give appropriate credit to the original author(s) and the source, provide a link to the Creative Commons licence, and indicate if changes were made. The images or other third party material in this article are included in the article's Creative Commons licence, unless indicated otherwise in a credit line to the material. If material is not included in the article's Creative Commons licence and your intended use is not permitted by statutory regulation or exceeds the permitted use, you will need to obtain permission directly from the copyright holder. To view a copy of this licence, visit <http://creativecommons.org/licenses/by/4.0/>.

## References

- Abdollahi A, Arias I (2012) Numerical simulation of intergranular and transgranular crack propagation in ferroelectric polycrystals. *Int J Fract* 174(1):3–15. <https://doi.org/10.1007/s10704-011-9664-0>
- Akinbinu VA (2016) Class I and Class II rocks: implication of self-sustaining fracturing in brittle compression. *Geotech Geol Eng* 34:877–887. <https://doi.org/10.1007/s10706-016-0011-0>
- Ammouche A, Riss J, Breyse D, Marchand J (2001) Image analysis for the automated study of microcracks in concrete. *Cem Concr Compos* 23(2–3):267–278. [https://doi.org/10.1016/S0958-9465\(00\)00054-8](https://doi.org/10.1016/S0958-9465(00)00054-8)
- Bobet A, Einstein HH (1998) Fracture coalescence in rock-type materials under uniaxial and biaxial compression. *Int J Rock Mech Min Sci* 35(7):863–888. [https://doi.org/10.1016/S0148-9062\(98\)00005-9](https://doi.org/10.1016/S0148-9062(98)00005-9)
- Brace WF, Bombolakis EG (1963) A note on brittle crack growth in compression. *J Geophys Res* 68:3709–3713. <https://doi.org/10.1029/JZ068i012p03709>
- Brown ET (1981) Rock characterization, testing & monitoring: ISRM suggested methods. International Society for Rock Mechanics, Pergamon Press
- Cheng Y, Wong LNY (2018) Microscopic characterization of tensile and shear fracturing in progressive failure in marble. *J Geophys Res Solid Earth* 123(1):204–225. <https://doi.org/10.1002/2017JB014581>
- Cheng Y, Wong LNY, Maruvanchery V (2016) Transgranular crack nucleation in Carrara marble of brittle failure. *Rock Mech Rock Eng* 49(8):3069–3082. <https://doi.org/10.1007/s00603-016-0976-2>
- Conrad RE, Friedman M (1976) Microscopic feather fractures in the faulting process. *Tectonophysics* 33(1–2):187–198. [https://doi.org/10.1016/0040-1951\(76\)90056-1](https://doi.org/10.1016/0040-1951(76)90056-1)
- DiGiovanni A, Fredrich J, Holcomb D, Olsson W (2007) Microscale damage evolution in compacting sandstone. *Geol Soc Lond Spec Publ* 289(1):89–103. <https://doi.org/10.1144/SP289.6>
- Dyskin AV, Sahouryeh E, Jewell RJ, Joer H, Ustinov KB (2003) Influence of shape and locations of initial 3-D cracks on their growth in uniaxial compression. *Eng Fract Mech* 70(15):2115–2136. [https://doi.org/10.1016/S0013-7944\(02\)00240-0](https://doi.org/10.1016/S0013-7944(02)00240-0)
- Fairhurst CE, Hudson JA (1999) Draft ISRM suggested method for the complete stress-strain curve for intact rock in uniaxial compression. *Int J Rock Mech Min Sci* 36:279–289. [https://doi.org/10.1016/S0148-9062\(99\)00006-6](https://doi.org/10.1016/S0148-9062(99)00006-6)
- Fan LF, Gao JW, Du XL (2020a) Thermal cycling effects on micro-property variation of granite by a spatial micro-observation. *Rock Mech Rock Eng* 53(6):2921–2928. <https://doi.org/10.1007/s00603-020-02065-8>
- Fan L, Gao J, Du X, Wu Z (2020b) Spatial gradient distributions of thermal shock-induced damage to granite. *J Rock Mech Geotech Eng* 12(5):917–926. <https://doi.org/10.1016/j.jrmge.2020.05.004>
- Fan LF, Fan YD, Gao XY (2022) Spatial failure mode analysis of frozen sandstone under uniaxial compression based on CT technology. *Rock Mech Rock Eng*. <https://doi.org/10.1007/s00603-022-02859-y>
- Fourmeau M, Gomon D, Vacher R, Hokka M, Kane A, Kuokkala VT (2014) Application of DIC technique for studies of Kuru granite rock under static and dynamic loading. *Proc Mater Sci* 3:691–697. <https://doi.org/10.1016/j.mspro.2014.06.114>
- Fourmeau M, Kane A, Hokka M (2017) Experimental and numerical study of drill bit drop tests on Kuru granite. *Philos Trans Roy Soc A* 375(2085):20160176. <https://doi.org/10.1098/rsta.2016.0176>
- Ghamgosar M, Erarslan N, Williams DJ (2017) Experimental investigation of fracture process zone in rocks damaged under cyclic loadings. *Exp Mech* 57(1):97–113. <https://doi.org/10.1007/s11340-016-0216-4>
- Graham CC, Stanchits S, Main IG, Dresen G (2010) Comparison of polarity and moment tensor inversion methods for source analysis of acoustic emission data. *Int J Rock Mech Min Sci* 47(1):161–169. <https://doi.org/10.1016/j.ijrmms.2009.05.002>
- Guo BH, Dong HY (2019) Shear failure modes and AE characteristics of sandstone and marble fractures. *Open Geosci* 11(1):249–262. <https://doi.org/10.1515/geo-2019-0020>
- Hashiba K, Okubo S, Fukui K (2006) A new testing method for investigating the loading rate dependency of peak and residual rock strength. *Int J Rock Mech Min Sci* 43(6):894–904. <https://doi.org/10.1016/j.ijrmms.2005.12.005>
- He C, Okubo S, Nishimatsu Y (1990) A study of the class II behavior of rock. *Rock Mech Rock Eng* 23(4):261–273. <https://doi.org/10.1007/BF01043307>
- He MC, Zhao F, Cai M, Du S (2015) A novel experimental technique to simulate pillar burst in laboratory. *Rock Mech Rock Eng* 48(5):1833–1848. <https://doi.org/10.1007/s00603-014-0687-5>
- Herman JS, White WB (1985) Dissolution kinetics of dolomite: effects of lithology and fluid flow velocity. *Geochim Cosmochim Acta* 49(10):2017–2026. [https://doi.org/10.1016/0016-7037\(85\)90060-2](https://doi.org/10.1016/0016-7037(85)90060-2)
- Hoek E, Martin CD (2014) Fracture initiation and propagation in intact rock—a review. *J Rock Mech Geotech Eng* 6(4):287–300. <https://doi.org/10.1016/j.jrmge.2014.06.001>
- Hokka M, Black J, Tkalich D, Fourmeau M, Kane A, Hoang NH, Li CC, Chen WW, Kuokkala VT (2016) Effects of strain rate and confining pressure on the compressive behavior of Kuru granite. *Int J Impact Eng* 91:183–193. <https://doi.org/10.1016/j.ijimpeng.2016.01.010>
- Horii H, Nemat-Nasser S (1985) Compression-induced microcrack growth in brittle solids: axial splitting and shear failure. *J Geophys Res* 90(B4):3105–3125. <https://doi.org/10.1029/JB090iB04p03105>
- Janach W (1977) Failure of granite under compression. *Int J Rock Mech Min Sci Geomech Abstr* 14(4):209–215. [https://doi.org/10.1016/0148-9062\(77\)90950-0](https://doi.org/10.1016/0148-9062(77)90950-0)

- Kemeny JM, Cook NGW (1987) Crack models for the failure of rocks in compression. In: Desai CS, Krempf E, Kiousis PD, Kundu T (eds) *Constitutive laws for engineering materials: theory and applications*. Elsevier, Amsterdam, pp 879–887
- Kwiatk G, Goebel THW, Dresen G (2014) Seismic moment tensor and b value variations over successive seismic cycles in laboratory stick-slip experiments. *Geophys Res Lett* 41(16):5838–5846. <https://doi.org/10.1002/2014GL060159>
- Labuz JF, Biolzi L (1991) Class I vs Class II stability: a demonstration of size effect. *Int J Rock Mech Min Sci Geomech Abstr* 28(2–3):199–205. [https://doi.org/10.1016/0148-9062\(91\)92167-W](https://doi.org/10.1016/0148-9062(91)92167-W)
- Labuz JF, Zang A (2012) Mohr-Coulomb failure criterion. *Rock Mech Rock Eng* 45:975–979. <https://doi.org/10.1007/s00603-012-0281-7>
- Li CC (2011) Chapter 18: rock support for underground excavations subjected to dynamic loads and failure. In: Zhou Y, Zhao J (eds) *Advances in rock dynamics and applications*. CRC Press, Boca Raton, pp 483–506
- Li CC (2019) Rockburst conditions and rockburst support. *Chin J Rock Mech Eng* 38(4):674–682. <https://doi.org/10.13722/j.cnki.jrme.2019.0125> (in Chinese)
- Li CC (2021) Principles and methods of rock support for rockburst control. *J Rock Mech Geotech Eng* 13(1):46–59. <https://doi.org/10.1016/j.jrmge.2020.11.001>
- Li CC, Zhang N, Ruiz J (2019) Measurement of the basic friction angle of planar rock discontinuities with three rock cores. *Bull Eng Geol Environ* 78(2):847–856. <https://doi.org/10.1007/s10064-017-1045-0>
- Litorowicz A (2006) Identification and quantification of cracks in concrete by optical fluorescent microscopy. *Cem Concr Res* 36(8):1508–1515. <https://doi.org/10.1016/j.cemconres.2006.05.011>
- Lockner DA, Byerlee JD, Kuksenko V, Ponomarev A, Sidorin A (1991) Quasi-static fault growth and shear fracture energy in granite. *Nature* 350(6313):39–42. <https://doi.org/10.1038/350039a0>
- Luo DN, Su GS, Zhang GL (2020) True-triaxial experimental study on mechanical behaviours and acoustic emission characteristics of dynamically induced rock failure. *Rock Mech Rock Eng* 53(3):1205–1223. <https://doi.org/10.1007/s00603-019-01970-x>
- Moore DE, Lockner DA (1995) The role of microcracking in shear-fracture propagation in granite. *J Struct Geol* 17(1):95–114. [https://doi.org/10.1016/0191-8141\(94\)E0018-T](https://doi.org/10.1016/0191-8141(94)E0018-T)
- Moradian ZA, Ballivy G, Rivard P, Gravel C, Rousseau B (2010) Evaluating damage during shear tests of rock joints using acoustic emissions. *Int J Rock Mech Min Sci* 47(4):590–598. <https://doi.org/10.1016/j.ijrmms.2010.01.004>
- Ohno K, Ohtsu M (2010) Crack classification in concrete based on acoustic emission. *Constr Build Mater* 24(12):2339–2346. <https://doi.org/10.1016/j.conbuildmat.2010.05.004>
- Pan PZ, Feng XT, Hudson JA (2006) Numerical simulations of Class I and Class II uniaxial compression curves using an elasto-plastic cellular automaton and a linear combination of stress and strain as the control method. *Int J Rock Mech Min Sci* 43(7):1109–1117. <https://doi.org/10.1016/j.ijrmms.2006.02.005>
- Park CH, Bobet A (2010) Crack initiation, propagation and coalescence from frictional flaws in uniaxial compression. *Eng Fract Mech* 77(14):2727–2748. <https://doi.org/10.1016/j.engfracmech.2010.06.027>
- Petit JP, Barquins M (1988) Can natural faults propagate under Mode II conditions? *Tectonics* 7(6):1243–1256. <https://doi.org/10.1029/TC007i006p01243>
- Saksala T, Hokka M, Kuokkala VT, Mäkinen J (2013) Numerical modeling and experimentation of dynamic Brazilian disc test on Kuru granite. *Int J Rock Mech Min Sci* 59:128–138. <https://doi.org/10.1016/j.ijrmms.2012.12.018>
- Saksala T, Gomon D, Hokka M, Kuokkala VT (2014) Numerical and experimental study of percussive drilling with a triple-button bit on Kuru granite. *Int J Impact Eng* 72:56–66. <https://doi.org/10.1016/j.ijimpeng.2014.05.006>
- Samaha HR, Hover KC (1992) Influence of microcracking on the mass transport properties. *ACI Mater J* 89(4):416–424. <https://doi.org/10.14359/2585>
- Tang CA, Kou SQ (1998) Crack propagation and coalescence in brittle materials under compression. *Eng Fract Mech* 61(3–4):311–324. [https://doi.org/10.1016/S0013-7944\(98\)00067-8](https://doi.org/10.1016/S0013-7944(98)00067-8)
- Tarasov BG, Stacey TR (2017) Features of the energy balance and fragmentation mechanisms at spontaneous failure of Class I and Class II rocks. *Rock Mech Rock Eng* 50:2563–2584. <https://doi.org/10.1007/s00603-017-1251-x>
- Tatami J, Yasuda K, Matsuo Y, Kimura S (1997) Stochastic analysis on crack path of polycrystalline ceramics based on the difference between the released energies in crack propagation. *J Mater Sci* 32(9):2341–2346. <https://doi.org/10.1023/A:1018588620081>
- Tkalich D, Fourmeau M, Kane A, Li CC, Cailletaud G (2016) Experimental and numerical study of kuru granite under confined compression and indentation. *Int J Rock Mech Min Sci* 87:55–68. <https://doi.org/10.1016/j.ijrmms.2016.05.012>
- Wang Y, Zhang H, Lin H, Zhao Y, Li X, Liu Y (2020) Mechanical behavior and failure analysis of fracture-filled gneissic granite. *Theor Appl Fract Mech* 108:102674. <https://doi.org/10.1016/j.tafmec.2020.102674>
- Whittaker BN, Singh RN, Sun G (1992) *Rock fracture mechanics. Principles, design and applications*. Elsevier, Netherlands
- Wong LNY, Einstein HH (2009) Crack coalescence in molded gypsum and Carrara marble: Part 1. Macroscopic observations and interpretation. *Rock Mech Rock Eng* 42(3):475–511. <https://doi.org/10.1007/s00603-008-0002-4>
- Yang SQ, Jiang YZ, Xu WY, Chen XQ (2008) Experimental investigation on strength and failure behavior of pre-cracked marble under conventional triaxial compression. *Int J Solids Struct* 45(17):4796–4819. <https://doi.org/10.1016/j.ijsolstr.2008.04.023>
- Yang SQ, Dai YH, Han LJ, Jin ZQ (2009) Experimental study on mechanical behavior of brittle marble samples containing different flaws under uniaxial compression. *Eng Fract Mech* 76(12):1833–1845. <https://doi.org/10.1016/j.engfracmech.2009.04.005>
- Zhang HJ, Li CC (2019) Effects of confining stress on the post-peak behaviour and fracture angle of Fauske marble and Iddefjord granite. *Rock Mech Rock Eng* 52(5):1377–1385. <https://doi.org/10.1007/s00603-018-1695-7>
- Zhang XP, Wong LNY (2013) Crack initiation, propagation and coalescence in rock-like material containing two flaws: a numerical study based on bonded-particle model approach. *Rock Mech Rock Eng* 46(5):1001–1021. <https://doi.org/10.1007/s00603-012-0323-1>
- Zhang CQ, Liu ZJ, Pan YB, Gao Y, Zhou H, Cui GJ (2020) Influence of amygdaloids on crack evolution and failure behavior of basalt. *Eng Fract Mech* 226:106843. <https://doi.org/10.1016/j.engfracmech.2019.106843>
- Zhou CS, Li KF, Pang XY (2012) Geometry of crack network and its impact on transport properties of concrete. *Cem Concr Res* 42(9):1261–1272. <https://doi.org/10.1016/j.cemconres.2012.05.017>

**Publisher's Note** Springer Nature remains neutral with regard to jurisdictional claims in published maps and institutional affiliations.